

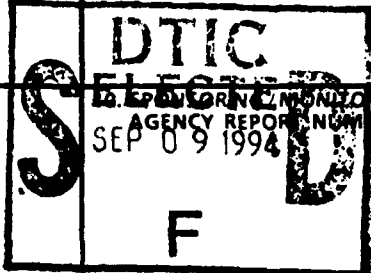


CITATION PAGE

Form Approved
OMB No. 0704-0188

4

ted to average 1 hour per response, including the time for reviewing instructions, searching existing data sources, reviewing the collection of information, send comments regarding this burden estimate or any other aspect of this burden to Washington Headquarters Services, Directorate for Information Operations and Reports, 1215 Jefferson Davis Highway, Suite 1204, Arlington, VA 22202-4302, and to the Office of Management and Budget, Paperwork Reduction Project (0704-0188), Washington, DC 20503.

1. AGENCY USE ONLY (Leave blank)		2. REPORT DATE August 26, 1994		3. REPORT TYPE AND DATES COVERED Final Technical 06/01/90-05/31/94	
4. TITLE AND SUBTITLE Microstructure and Crystal Defects in Perovskite Crystals with A-site Cation Ordering				5. FUNDING NUMBERS Contract No. N00014-90-J-1900	
6. AUTHOR(S) Dr. Edward Goo					
7. PERFORMING ORGANIZATION NAME(S) AND ADDRESS(ES) University of Southern California Department of Materials Science & Engineering Los Angeles, CA 90089-0241					
9. SPONSORING/MONITORING AGENCY NAME(S) AND ADDRESS(ES) Dr. Wallace A. Smith					
11. SUPPLEMENTARY NOTES					
12a. DISTRIBUTION AVAILABILITY STATEMENT Approved for Public Release. Distribution Unlimited				12b. DISTRIBUTION CODE	
13. ABSTRACT (Maximum 200 words) Microstructure of ordered A-site perovskites has been studied by transmission electron microscopy and electron diffraction. Determination of the diffuseness of the ferroelectric phase transition as a function of temperature allow the diameter of the microregions (Kanzig regions) to be determined. <div style="text-align: right;">DTIC QUALITY INSPECTED 3</div>					
14. SUBJECT TERMS ferroelectrics, perovskites, microstructure				15. NUMBER OF PAGES 4	
				16. PRICE CODE	
17. SECURITY CLASSIFICATION OF REPORT Unclassified	18. SECURITY CLASSIFICATION OF THIS PAGE Unclassified	19. SECURITY CLASSIFICATION OF ABSTRACT Unclassified	20. LIMITATION OF ABSTRACT UL		

Final Progress Report

A summary of the major results of the research grant entitled "Microstructure and Crystal Defects in Perovskite Crystals with A-site Cation Ordering" is presented. To keep the report short an appendix containing reprints and preprints of publications resulting from the research is attached at the end of the report. The reader can refer to the publications which contain most of the data resulting from this project.

The microstructure of a large number of a-site complex perovskites were studied. Ordering of the a-site cations were found in the following systems: $(\text{Pb,Ca})\text{TiO}_3$, $(\text{Ba,Ca})\text{TiO}_3$ and $(\text{Sr,Ca})\text{TiO}_3$. Ordering was not found in: $(\text{Pb,Ba})\text{TiO}_3$, $(\text{Pb,Sr})\text{TiO}_3$ and $(\text{Ba,Sr,Pb})\text{TiO}_3$. We believe is not coincidental that CaTiO_3 is present in all the systems that undergo chemical ordering. CaTiO_3 undergoes a transformation to a superlattice that is easily described as due to tilting of the oxygen octahedra.¹ The superlattice is responsible for the $1/2\langle 110 \rangle$ and $1/2\langle 100 \rangle$ superlattice reflections. The tilting favors ordering of the a-site cations because it causes some of the a-sites to increase in size while others decrease in size. The ordering of a-site cations cause the $1/2\langle 111 \rangle$ superlattice reflection. Hot stage TEM data show that the $1/2\langle 110 \rangle$ and $1/2\langle 100 \rangle$ reflections disappear upon heating at a relative low temperature. The $1/2\langle 111 \rangle$ reflections do not disappear upon heating up to a temperature of 950°C the maximum temperature at which these measurements may be done with our apparatus.

We also studied the paraelectric - ferroelectric transitions in these systems by measuring the dielectric constant vs temperature. Since PbTiO_3 has a high Curie point of 490°C we had to design system allowing measurements at these temperatures. Most setups are limited to 300°C due to the use of organic insulators. In our setup all of the insulators are alumina and the maximum operating temperature is limited by the melting point of the copper conductor. We have routinely done measurements to 500°C with no observed ill effects on the apparatus.

94-29393



1

84 9 07 19 8

A diffuse phase transition is observed in all of the complex perovskites. In systems such as $(\text{Pb,Ba})\text{TiO}_3$ where a complete solid solution exist and there is no cation ordering we were able to measure how the diffuseness of the transition varies with composition. We have shown that this data can in turn be used to calculate the diameter of the chemically inhomogeneous microregions(Kanzig regions)² that are responsible for the diffuse transition. This is the first experimental method for measuring the Kanzig region diameter. Our data from the $(\text{Pb,Ba})\text{TiO}_3$ system indicate the Kanzig regions are 20-40 Å in diameter.

1. "Powder Neutron diffraction Study of the Perovskites CaTiO_3 and CaZrO_3 ," H. J. A. Koopmans, G. M. H. van de Velde and P. J. Gellings, Acta Cryst., **C39**, pp 1323-1325 (1983)
2. "A Quantitative Analysis of the Size of the Kanzig Regions," R. Ganesh and E. Goo (accepted for publication in J. Mater. Sci. Lett.)

Accession For		
NTIS	GRA&I	<input checked="" type="checkbox"/>
DTIC	AB	<input type="checkbox"/>
U.S. GOVT		<input type="checkbox"/>
J. Mater. Sci.		

Publications Resulting from Research Support

"Microstructure and Crystal Structure Investigations in Lead Calcium Titanates and Lead Strontium Titanates," K. Ananth, R. Ganesh and E. Goo, **Ceramic Transactions**, Dielectric Ceramics: Processing, Properties and Applications, eds. K. M Nair, J. P. Guha and A. Okamoto, vol. 32, American Ceramic Society, Westerville, OH, (1993) 145-54

"Observation of Crystal and Domain Structure in $(\text{Pb}_x\text{Ba}_{1-x})\text{TiO}_3$," S. Sudhakar, R. Ganesh and E. Goo, **Ceramic Transactions**, Dielectric Ceramics: Processing, Properties and Applications, eds. K. M Nair, J. P. Guha and A. Okamoto, vol. 32, American Ceramic Society, Westerville, OH, (1993) 139-143

"A Quantitative Analysis of the Size of the Kanzig Regions," R. Ganesh and E. Goo (accepted for publication in J. Mater. Sci. Lett.)

"Microstructure and Dielectric Characteristics of $(\text{Pb}_x\text{Ba}_{x-0.5}\text{Sr}_{0.5})\text{TiO}_3$ Ceramics," R. Ganesh and E. Goo (submitted for publication to the J. of the Am. Ceram. Soc.)

"Dielectric Properties and Microstructural Characterization of $(\text{Ba}_x\text{Ca}_{1-x})\text{TiO}_3$," S. Sudhakar and E. Goo (submitted for publication to the J. of Mater. Sci.)

"Microstructural and Dielectric Properties of $(\text{Pb},\text{Ba})\text{TiO}_3$," S. Sudhakar and E. Goo (in preparation)

Participants in the Research Project

Mr. R. Ganesh is a fifth year graduate student and is currently writing his Ph.D. thesis. He is expected to graduate by January 1995.

Mr. S. Sudhakar is a fifth year graduate student and is finishing up his thesis. He is expected to graduate by November 1994.

Mr. K. Ananth participated in the project for one year before switching to another adviser.

Appendix

Reprints and Preprints of Publications

OBSERVATION OF CRYSTAL AND DOMAIN STRUCTURE IN (Pb_{1-x}Ba_x)TiO₃

Sudhakar Subrahmanyam, Ramaratnam Ganesh and Edward Goo,
Department of Materials Science and Engineering, University of Southern
California, Los Angeles, CA 90089-0241.

ABSTRACT

The crystal and domain structure of (Pb_{1-x}Ba_x)TiO₃ ($0 \leq x \leq 0.5$) have been investigated by x-ray diffraction and transmission electron microscopy. The crystal structure has been determined to be tetragonal with c/a ratio increasing with increasing value of x . Ferroelectric domains have been observed by TEM. The orientation of the 90° domain boundary walls along the {101} crystallographic plane and the presence of 180° domain walls have further been confirmed by TEM studies for $x = 0.1, 0.2$.

I. Introduction

Very little work has been done on A-site substituted perovskites. Barium titanate is a widely used perovskite for its dielectric and piezoelectric properties. Lead titanate possesses a large spontaneous polarization. However, its large c/a ratio has limited its application. A solid solution exists between BaTiO₃ and PbTiO₃^{1,2} although very little is known about these compositions. The (Pb_{1-x}Ba_x)TiO₃ is potentially an excellent system for dielectric and piezoelectric applications.

In the present study, the crystal structure and domain structure in (Pb_{1-x}Ba_x)TiO₃ were studied by x-ray diffraction and transmission electron microscopy.

II. Experimental Procedure

The compositions of the samples is (Pb_{1-x}Ba_x)TiO₃, where $x = 0.1, 0.2$,

To the extent authorized under the laws of the United States of America, all copyright interests in this publication are the property of The American Ceramic Society. Any duplication, reproduction, or republication of this publication or any part thereof, without the express written consent of The American Ceramic Society or fee paid to the Copyright Clearance Center, is prohibited.

0.3, 0.4 and 0.5. These compositions refer to the relative amounts of oxides used in preparing the powder and do not represent the final composition of the sintered product. Bulk processing of the perovskite powder was done with chemically pure PbO (99.5%), TiO_2 (99.7%), and BaCO_3 (99.5%). Stoichiometric amounts of the powders were mixed by ball milling with alumina balls and distilled water (in the form of a slurry) for 5 h. in a polyethylene container and oven dried. The powder was then calcined in an alumina crucible at 850°C for 5 h. After remilling again for 5 h followed by drying, the final product was ground with a mortar and pestle into a fine powder. The powders were then cold pressed at a pressure of 240 MPa (35,000 psi) into disks 3mm thick and 25 mm diameter. The compacts were then sintered in the temperature range 1250°C - 1350°C for 5 h.

X-ray samples were obtained by cutting a thin slice from the as-sintered samples and mechanically polishing with a final polish in $0.3\text{-}\mu\text{m}$ alumina slurry to give a smooth surface. Lattice parameters were measured by using a powder X-ray diffractometer*, using $\text{Cu K}\alpha$ X-rays, operating at 35 kV and 50 mA.

Transmission electron microscopy (TEM) samples were obtained by ultrasonically drilling the sintered samples into 3-mm disks. The disks were mechanically polished and dimpled to $20\text{-}\mu\text{m}$ and then ion-milled with argon ions. TEM was done on a microscope* operating at an accelerating voltage of 120 kV.

III. Results and Discussion

(1) Crystal Structure

It has been reported previously³ that both BaTiO_3 and PbTiO_3 have a tetragonal structure at room temperature with c/a ratio of 1.029 and 1.061 respectively. In the present study, it has been verified that the crystal structure of $(\text{Pb,Ba}_{1-x}\text{TiO}_3)$ remains tetragonal over the composition range $0 \leq x \leq 0.5$. The indexed x-ray diffraction peaks and their corresponding 2-theta values were used to calculate the lattice parameters using the method of least

* Rigaku Co., Tokyo, Japan

* EM 420, Phillips Electronic Instruments, Mahwah, NJ.

squares. The lattice parameters a and c decreased and increased respectively with increasing lead content. This is in agreement with interpolating the a and c values for PbTiO_3 and BaTiO_3 . The density* increased with increasing lead content (Table I). The experimental density (ρ_{ex}) was always greater than 85% of the theoretical density (ρ_{th}). The cell volume ($V = a^2c$) did not show any significant trend over the range measured. Also, x-ray diffraction and electron diffraction did not reveal any ordered peaks.

TABLE I

Lattice Parameters and Density of $(\text{Pb,Ba}_{1-x})\text{TiO}_3$

Composition 'x'	0	0.1	0.2	0.3	0.4	0.5
Molecular Weight (gms)	233.20	240.18	247.17	254.16	261.15	268.14
$a(\text{\AA})$	3.999	3.984	3.977	3.970	3.967	3.939
$c(\text{\AA})$	4.039	4.032	4.042	4.054	4.063	4.059
c/a	1.010	1.012	1.016	1.021	1.024	1.030
Cell Volume (\AA^3)	64.591	63.996	63.930	63.894	63.939	62.978
ρ_{ex} (gm/cm ³)	5.613	5.677	5.761	5.859	5.973	6.134
ρ_{th} (gm/cm ³)	6.009	6.231	6.419	6.604	6.781	7.068
$\rho\%$	93.40	91.10	89.74	88.71	88.08	86.77

(2) Observation of Domain Structure by Transmission Electron Microscopy

Ferroelectric domains have been observed in the compositions $x = 0.1, 0.2$. Both 90° and 180° domain boundaries were seen [Fig. 1]. The 90° boundary walls lie on the $\{101\}$ planes, and tend to be straight. However, the energy of the 180° boundary walls is less sensitive to crystallographic orientation. Hence they appear 'wavy'. The SADP of the $\langle 100 \rangle$ zone axis in the composition $x = 0.2$ show spot splitting in the region of the 90° domains

* Experimental density (ρ_{ex}) = (Weight of sample in air) / (Loss of weight of sample in water)
Theoretical density (ρ_{th}) = $\frac{(\text{Number of molecules/unit cell}) (\text{Molecular weight of } (\text{Pb,Ba}_x)\text{TiO}_3)}{(\text{Avogadro's number}) (\text{Volume of the unit cell})}$

(Fig. 2a). Fig. 2b shows the dark field image for $g = [011]$ close to the $\langle 100 \rangle$ zone axis region. The spot splitting is consistent with the presence of 90° domains.

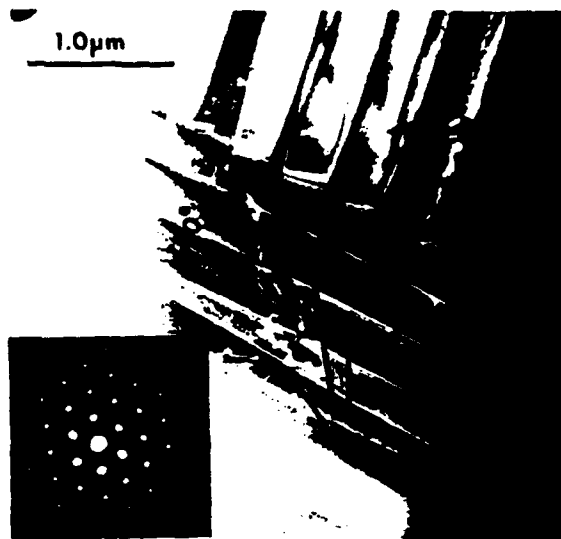


Fig. 1. Dark field micrograph taken with $\{110\}$ type reflection from $[111]$ zone axis showing the 90° domain walls oriented along the (101) plane. 180° domains can also be seen.

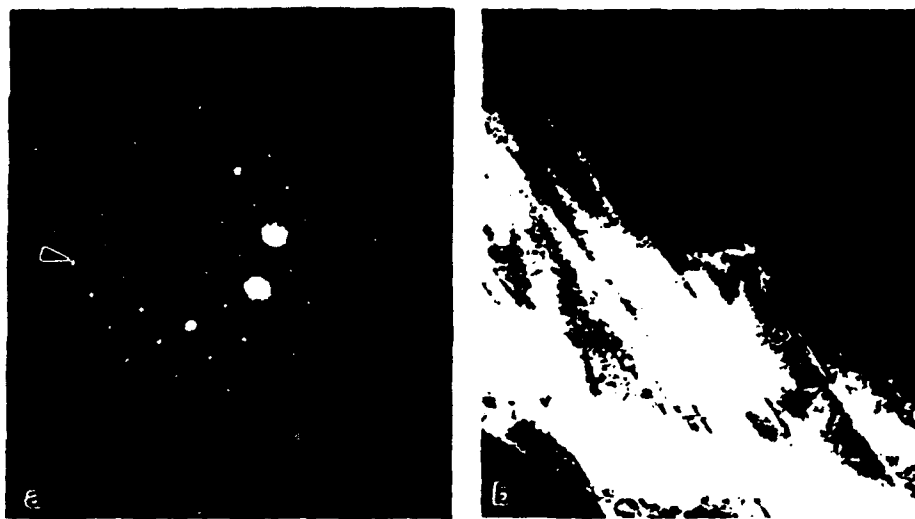


Fig. 2. (a) The two beam condition from the $\{110\}$ type reflection in the $[100]$ zone axis, showing spot splitting in the region of the 90° domains. (b) Dark-field of the same region.

IV. Conclusion

Crystal structure and domain structure of $(\text{Pb}_x\text{Ba}_{1-x})\text{TiO}_3$, with x ranging from 0.1 to 0.5 were investigated by x-ray diffraction and transmission electron microscopy. The crystal structure was determined to be tetragonal with the lattice parameters a and c decreasing and increasing respectively with increasing lead content. The density increases with increasing lead content. 90° and 180° domains were observed in $x = 0.1, 0.2$ compositions with the 90° domains oriented along the $\{101\}$ crystallographic plane. The domain structure was similar to that of BaTiO_3 ⁴.

Acknowledgements: The authors acknowledge the use of the facilities at the Center of Electron Microscopy and Microanalysis (CEMMA) at USC.

References

1. Malcolm McQuarrie, "Studies in the System $(\text{Ba,Ca,Pb})\text{TiO}_3$," *J. Am. Ceram. Soc.*, **40** [2] 35-41 (1957)
2. Takuro Ikeda, "Some Studies on the Ternary System $(\text{Ba-Pb-Ca})\text{TiO}_3$," *J. Phys. Soc. Japan*, **13** [4] 335-340 (1958)
3. Francis S. Galasso, "Structure, Properties and Preparation of Perovskite-Type Compounds," pp. 18-19. Volume 5, Pergamon Press, Oxford, 1969.
4. Yung H. Wu, Helen M. Chan, Zhang Xiao Wen, and Martin P. Harmer, "Scanning Electron Microscopy and Transmission Electron Microscopy Study of Ferroelectric Domains in Doped BaTiO_3 ," *J. Am. Ceram. Soc.*, **69** [8] 594-602 (1986).

MICROSTRUCTURE AND CRYSTAL STRUCTURE INVESTIGATIONS IN LEAD CALCIUM TITANATES AND LEAD STRONTIUM TITANATES

Kartik Ananth, Ramaratnam Ganesh and Edward Goo, Department
of Materials Science and Engineering, University of Southern California, Los
Angeles, CA-90089-0241

ABSTRACT

The microstructure and crystal structure of $(\text{Pb}_x\text{Ca}_{1-x})\text{TiO}_3$ and $(\text{Pb}_x\text{Sr}_{1-x})\text{TiO}_3$ were investigated. The compositions with varying x in the $(\text{Pb}_x\text{Sr}_{1-x})\text{TiO}_3$ and the calcium rich region ($x < 0.5$) in the $(\text{Pb}_x\text{Ca}_{1-x})\text{TiO}_3$ system, were prepared by standard bulk powder processing techniques.

X-ray diffraction studies indicated that the $(\text{Pb}_x\text{Sr}_{1-x})\text{TiO}_3$ has a tetragonal crystal structure for $x \geq 0.5$ and cubic for the other compositions. In the lead calcium system the crystal structure for the $x = 0.4, 0.3$ was tetragonal with a c/a ratio very close to 1 and orthorhombic for other compositions. In both systems it was found that the c/a ratio decreased with decreasing lead content in the A site. Microstructural investigations by TEM studies showed the presence of domains in the lead strontium system and the presence of anti-phase boundaries and ordering in the $(\text{Pb}_x\text{Ca}_{1-x})\text{TiO}_3$ compositions.

INTRODUCTION

Perovskite systems (ABO_3) have been studied widely for B site substitutions^{1,2}, but relatively less work has been done on the A site.

Interest in these systems is due to their potential as ferroelectric materials with high dielectric and piezoelectric constants. Lead titanate has a perovskite crystal structure, with a relatively high Curie point of 490°C and good piezoelectric properties³. However, due to the large c/a ratio in PbTiO_3 (1.061) in the low temperature tetragonal phase, it disintegrates into powder when cooled through the Curie point³. The present study aims at a structure property correlation through X-ray and electron microscopic investigations in $(\text{Pb}_x\text{Ca}_{1-x})\text{TiO}_3$ and $(\text{Pb}_x\text{Sr}_{1-x})\text{TiO}_3$ systems.

To the extent authorized under the laws of the United States of America, all copyright interests in this publication are the property of The American Ceramic Society. Any duplication, reproduction, or republication of this publication or any part thereof, without the express written consent of The American Ceramic Society or fee paid to the Copyright Clearance Center, is prohibited.

EXPERIMENTAL PROCEDURE

Conventional powder processing techniques were employed to prepare the bulk powders. These involved weighing stoichiometric amounts of the chemically pure PbO (99.5 %), TiO_2 (99.7 %), CaCO_3 (99.5%) and SrCO_3 (99.5 %). These were then ball milled with Alumina balls for 5 hours in deionized water, followed by oven drying of the filtrate residue. The ceramic powders were then calcined at 850 °C for 5 hours in a covered alumina crucible. The calcined residue was ball milled again and the final product was ground using a mortar and pestle into a fine powder. The calcined powders were then cold pressed in a hydraulic press at 35,000 psi into cylindrical pellets with 25 mm diameter and 3 mm thickness. The compacts were then sintered at 1200 °C for 5 hours.

For the $(\text{Pb}_{1-x}\text{Ca}_x)\text{TiO}_3$ perovskite compositions of $x < 0.5$ were prepared in decrements of 0.1. For the $(\text{Pb}_{1-x}\text{Sr}_x)\text{TiO}_3$ system compositions starting from $x = 0.9$ to $x = 0.1$ in decrements of 0.1 were prepared.

For X-ray diffraction studies a mechanically polished as sintered specimen was used. X-ray studies were done using a diffractometer* using $\text{Cu K}\alpha$ radiation and operating at 35 kV and 50 mA.

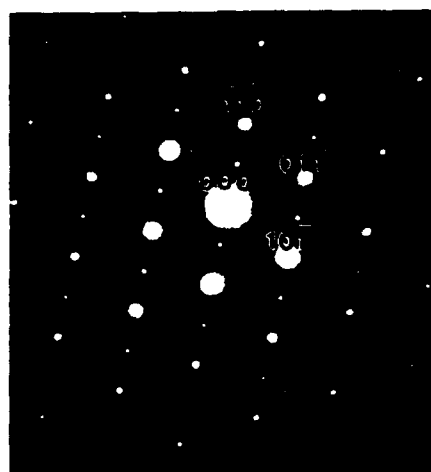
TEM samples were prepared from the sintered product by cutting 3mm diameter circular disks using an ultrasonic drill. This was further mechanically polished and dimpled to 20 microns thickness. These were then mounted on a Cu grid and milled using Ar ions. TEM studies were done on a microscope** operating at an accelerating voltage of 120 kV.

RESULTS AND DISCUSSION

X-ray diffraction studies were done for all the samples prepared. XRD studies done on $(\text{Pb}_{1-x}\text{Ca}_x)\text{TiO}_3$ indicated the crystal structure to be cubic for $x = 0.4$ and 0.3 and orthorhombic for other compositions. However, TEM studies done for $x = 0.4, 0.3$ compositions showed the presence of superlattice reflections in only one direction along the $[111]$ zone axis, as shown in fig. 1.

* Rigaku Co., Tokyo, Japan

** EM 420, Phillips Electronic Instruments, Mahwah, NJ



(a)



(b)



(c)



(d)

Fig. 1. Electron Diffraction patterns for (a) $[111]$ zone axis (b) $[110]$ zone axis (c) $[100]$ zone axis having both $1/2\{110\}$ and $1/2\{100\}$ reflections (d) $[100]$ zone axis having $1/2\{110\}$ reflections.

This contradicts the results obtained by X-ray measurements as a cubic material should have three fold symmetry along the [111] direction. It was reported in earlier studies^{4,7}, that the c/a ratio decreases with increasing Ca content. This is reasonable to expect because CaTiO_3 has a lower c/a ratio than PbTiO_3 (the crystal structure however, is different). Further, the [100] zone axis pattern in the $x = 0.3, 0.4$ compositions exhibited four fold symmetry. Therefore, it's concluded that for $x = 0.3$ and 0.4 the crystal structure is tetragonal with the c/a value close to unity, making it difficult to resolve the peak splitting in the X-ray scan. This is further corroborated by the fact that any material with a cubic crystal structure cannot be ferroelectric but $(\text{Pb}_{0.3}\text{Ca}_{0.7})\text{TiO}_3$ was found to be ferroelectric as it exhibited a hysteresis loop. The crystal structure results for $(\text{Pb}_x\text{Ca}_{1-x})\text{TiO}_3$ in the calcium rich region are summarized Table 1.

X	Crystal Structure	Lattice parameters (Å)
0.1	Orthorhombic	$a=5.42, b=7.657, c=5.372$
0.2	Orthorhombic	$a=5.44, b=7.69, c=5.40$
0.3	Tetragonal	$c/a=1$
0.4	Tetragonal	$c/a=1$

Table 1. Crystal structure and lattice parameters for $(\text{Pb}_x\text{Ca}_{1-x})\text{TiO}_3$

Crystal structure investigations in $(\text{Pb}_x\text{Sr}_{1-x})\text{TiO}_3$ indicated that the crystal structure was tetragonal in the lead rich regions ($x > 0.4$) and cubic for other compositions ($x \leq 0.4$). This is expected as the crystal structure of PbTiO_3 at room temperature is tetragonal with a c/a value of 1.061 and that of SrTiO_3 is cubic.

The crystal structure data for the lead strontium compositions are summarized in Table 2.

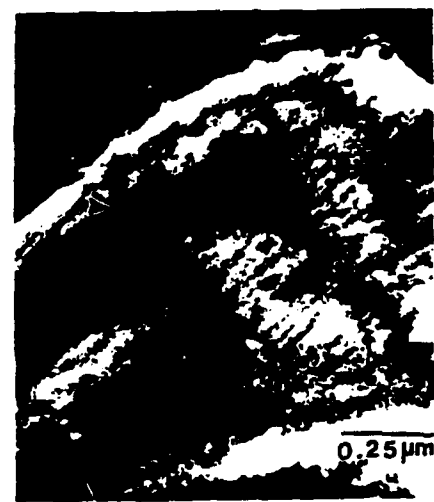
x	c/a	c	a	structure
0.9	1.0435	4.004	3.837	Tetragonal
0.8	1.0307	3.983	3.864	Tetragonal
0.7	1.0206	3.9838	3.9032	Tetragonal
0.6	1.0166	3.9472	3.8828	Tetragonal
0.5	1.0164	3.9606	3.8964	Tetragonal
0.4	1.0000	3.9278	3.9278	Cubic
0.3	1.0000	3.9434	3.9434	Cubic
0.2	1.0000	3.8807	3.8807	Cubic
0.1	1.0000	3.8804	3.8804	Cubic

Table 2. Crystal structure and lattice parameters for $(\text{Pb}_x\text{Sr}_{1-x})\text{TiO}_3$

TEM studies done on $(\text{Pb}_x\text{Ca}_{1-x})\text{TiO}_3$ ($x < 0.5$) indicated that these materials have an ordered structure as superlattice reflections of the type



(a)



(b)



(c)



(d)

Fig. 2. Dark field images for (a) $1/2(111)$ (b) (111) (c) (010) (d) (101)

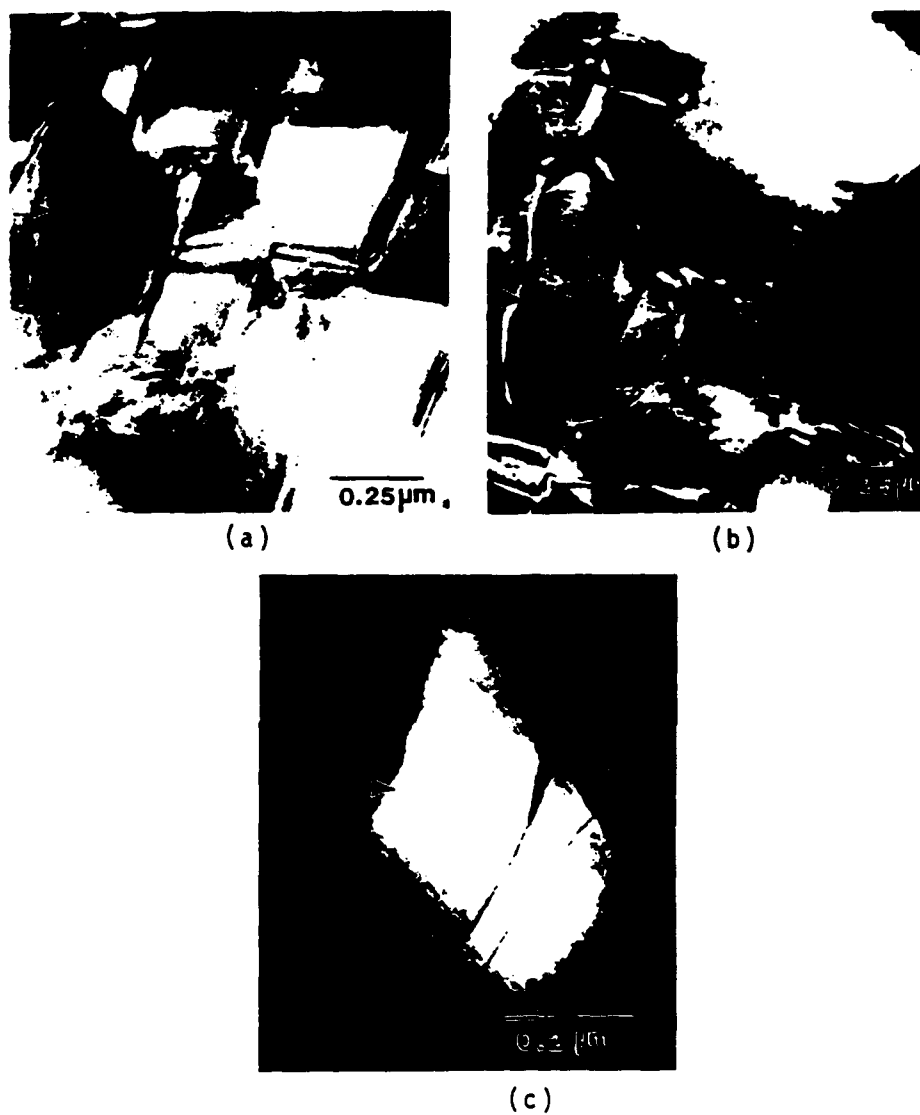


Fig. 3. Dark field images for one variant using different superlattice reflections: (a) $1/2(110)$; zone axis $[111]$ (b) $1/2(111)$; zone axis $[110]$ (c) $1/2(010)$; $[100]$ zone axis



Fig. 4. Transmission electron micrograph showing the existence of 90° domains and 180° domains in $(\text{Pb,Sr}_{1-x})\text{TiO}_3$

$1/2\{100\}$, $1/2\{110\}$ and $1/2\{111\}$ were observed in the diffraction pattern as shown in fig. 1. Dark field studies were done on the various samples to find out the origin of the superlattice reflections and to see if it was different from that obtained for the lead rich compositions. In fig. 2, it is seen that the two variants, indicated by the arrows, are clearly imaged for the $1/2\{111\}$ reflection and entirely absent for the bulk reflections. This confirms that the superlattice reflections are of a different origin than the bulk reflections. Presence of anti-phase boundaries is also evidenced as shown in fig. 2a. Dark field images using different superlattice reflections are shown in fig. 3. It is observed that the region shown by the arrow is clearly seen when imaged with $1/2\{100\}$, $1/2\{110\}$, and $1/2\{111\}$ superlattice reflections. This indicates that the different superlattice reflections are of the same origin unlike⁴ what was observed for the $x > 0.5$ compositions. Hence, it is possible that a different kind of ordering exists for the calcium rich compositions in $(\text{Pb}_x\text{Ca}_{1-x})\text{TiO}_3$. Presence of superlattice reflections were observed for the $x = 0.1$ and $x = 0.2$ compositions as well, but they were not significantly different from what was observed for other compositions.

TEM studies on $(\text{Pb}_x\text{Sr}_{1-x})\text{TiO}_3$ indicated that these materials do not have an ordered structure, as no superlattice reflections were present in the diffraction patterns. However, dark field studies showed the presence of domains in the composition range $x = 0.3$ to 0.9 . These are indicative of the material having a pseudo cubic crystal structure even in the strontium rich regions of $x = 0.4$ and 0.3 , although the X-ray diffraction studies showed a cubic structure for these compositions. The probable structure for $x = 0.4$ and 0.3 compositions is also tetragonal, with a c/a ratio very close to one. The domains seen in the microstructure are 90 degree domains lying along the (101) planes. 180 degree domains are also seen as shown in fig. 4., they do not have a preferred planar orientation as there is no elastic strain energy change during their formation.

CONCLUSIONS

Crystal structure and microstructural studies in $(\text{Pb}_x\text{Ca}_{1-x})\text{TiO}_3$ ($x < 0.5$) and $(\text{Pb}_x\text{Sr}_{1-x})\text{TiO}_3$ ($x = 0.1$ to 0.9) are reported.

In the $(\text{Pb}_x\text{Ca}_{1-x})\text{TiO}_3$ system it is concluded that ordering exists for these compositions since superlattice reflections of the type $1/2\{100\}$, $1/2\{110\}$, $1/2\{111\}$ were clearly evidenced. Studies also indicate that the crystal structure is orthorhombic for $x = 0.1$ and 0.2 and tetragonal for other compositions. Hysteresis measurements done on the $x = 0.3$ composition

indicate that the material is ferroelectric.

In the $(\text{Pb}_x\text{Sr}_{1-x})\text{TiO}_3$ system it is found that the lead rich region ($x > 0.4$) has a tetragonal crystal structure and the strontium rich region ($x \leq 0.4$) has a pseudo-cubic crystal structure for $x = 0.4$ and 0.3 , and a cubic structure for other compositions. Domains are seen and reported in the composition range of $x = 0.3$ to 0.9 . The 90 degree domains are oriented preferentially along the (101) planes, there is no particular orientation for the 180 degree domains. No ordering is present in the $(\text{Pb}_x\text{Sr}_{1-x})\text{TiO}_3$ system.

ACKNOWLEDGEMENTS

The authors would like to thank the Center for Electron Microscopy and Microanalysis (CEMMA) for the use of its facilities.

REFERENCES

- [1] F.S.Galasso and J.Pyle, "Ordering in Compounds of the $A(\text{B}'_{0.33}\text{Ta}_{0.67})\text{O}_3$ Type", *Inorg. Chem.*, 2 [3] 482 (1963)
- [2] X.Zhang, Q.Wang and B.Gu, "Study of the Order- Disorder Transition in $A(\text{B}'\text{B}')\text{O}_3$ Perovskite Type Ceramics", *J.Am.Ceram.Soc.*, 74 [11] 2846-50 (1991)
- [3] B.Jaffe, R.Cook and H.Jaffe, *Piezoelectric ceramics*; 115-18 Academic Press, New York, 1971
- [4] E.Sawaguchi, T.Mitsuma and Z.Ishii, "Double Hysteresis Loop of $(\text{Pb}_x\text{Ca}_{1-x})\text{TiO}_3$ Ceramics", *J.Phy.Soc.Jpn.*, 11 1298 (1956)
- [5] E.Sawaguchi and M.L.Charters, "Aging and the Double Hysteresis Loop of $(\text{Pb}_x\text{Ca}_{1-x})\text{TiO}_3$ Ceramics", *J.Am.Ceram.Soc.*, 42 [4], 157-164 (1959)
- [6] G.King and E.Goo, "Effect of the c/a Ratio on the Domain Structure in $(\text{Pb}_x\text{Ca}_{1-x})\text{TiO}_3$ ", *J.Am.Ceram.Soc.*, 73 [6] 1534-39 (1990)
- [7] G.King, E.Goo, T.Yamamoto and K.Okazaki, "Crystal Structure and Defects of Ordered $(\text{Pb}_{1-x}\text{Ca}_x)\text{TiO}_3$ ", *J.Am.Ceram.Soc.*, 71 [6] 454-60 (1988)

A QUANTITATIVE ANALYSIS OF THE SIZE OF THE KANZIG REGIONS

Ramaratnam Ganesh and Edward Goo

Department of Materials Science and Engineering, University of Southern California,

Los Angeles, California 90089

Diffuse paraelectric to ferroelectric phase transitions in ceramics forming solid solutions are attributed to statistical fluctuations in composition [1-3] in submicron regions, known as Kanzig regions [4]. These fluctuations in compositions become larger the smaller the Kanzig region. These size of the Kanzig region represent the critical size that is needed to transform to a ferroelectric state on cooling through the Curie point. Due to the dependence of the Curie temperature on composition, microregions of differing composition have different local Curie temperatures. A Gaussian distribution of Curie temperatures of the microregions explains the diffuse phase transition observed. A general feature of materials exhibiting diffuse phase transitions is the random occupation of ions of different types in crystallographically equivalent positions. Ordering of atoms tend to minimize such fluctuations in compositions resulting in a sharp transition from the paraelectric to ferroelectric phase [5].

The size of the Kanzig regions is an important parameter that controls the width of the transition range. Smaller the size of the Kanzig region greater is the width of the transition range. Earlier treatments on the size of the Kanzig regions have been qualitative in nature and no experimentally evaluated results have been reported. The size of the Kanzig region is of paramount importance in ferroelectrics with diffuse phase transitions. In this paper, we present a quantitative model to experimentally determine the size of the

Kanzig region.

Quantitative analysis of the influence of composition fluctuations on diffuse phase transitions for solid solutions of two compounds with perovskite structures was reported by Smolensky [1]. Consider a solid solution of the form $A'_x A''_{1-x} BO_3$. The A-site atoms are located in a polyhedra with 12-fold coordination and the B-site atoms occupy the octahedral positions. In a microregion consisting of n molecules of $A'BO_3$ and $A''BO_3$ the probability of finding m molecules of $A'BO_3$ in the absence of ordering of any sort is given by [6]

$$P(m) = \frac{1}{\sqrt{2\pi n x(1-x)}} \exp\left[-\frac{n\xi^2}{2x(1-x)}\right] \quad (1)$$

ξ gives the amount by which the microscopic concentration differs from macroscopic concentration and is given by $\xi = q - x$ where, $q = m/n$. $P(m)$ is a maximum at $\xi = 0$, therefore, the value of ξ at half the maximum value is given by,

$$\exp\left[-\frac{n\xi^2}{2x(1-x)}\right] = \frac{1}{2} \quad (2)$$

Solving for ξ , we have

$$\xi = \pm \sqrt{\frac{x(1-x) \ln 4}{n}} \quad (3)$$

The negative value of ξ in the above equation is neglected as the curve is symmetrical about the maxima. For small fluctuations in composition the change in the Curie point is assumed to vary linearly with concentration change. Therefore, $\xi = \nu(T - T_0)$ where, ν is a

proportionality constant, T is the Curie temperature of the microregion and T_0 is the macroscopic Curie temperature. Statistically the number of Kanzig regions that have compositions close to the mean composition is a maximum. Hence, T_0 represents the temperature at which maximum number of Kanzig regions undergo a transformation into a ferroelectric phase. In other words, at T_0 , Kanzig regions corresponding to $\xi=0$ transform into the ferroelectric state from the paraelectric state. Therefore, the spread in the transition region (Δ) with respect to temperature for a curve centered at T_0 is given by,

$$\Delta = \frac{1}{v} \sqrt{\frac{x(1-x) \ln 4}{n}} \quad (4)$$

The above equations are valid for temperatures greater than the Curie temperature and Δ represents the width of the transition region above the Curie point and at half the maximum value of the dielectric constant at a particular frequency. A typical plot of the dielectric constant versus temperature curve is shown in Figure 1. for a diffuse phase transition. The value of Δ is indicated on the curve.

[Fig. 1. Approximately here.]

From the above equation it is possible to measure the size of the Kanzig regions by using the value of Δ calculated from the dielectric constant versus temperature curve for a particular composition and frequency. The value of v in such a case may be obtained by interpolating the Curie temperature of the given composition with the Curie temperatures of the pure compositions. However, to minimize the errors involved, the following procedure is adopted. Experimentally calculated values of Δ are plotted as a function composition. The

value of ν is obtained from a plot of T_0 as a function of x for a range of compositions. The value of ν , thus calculated, is incorporated in equation (4) and the value of n varied to obtain a best fit with the experimentally calculated values of Δ .

ACKNOWLEDGEMENT

This work was supported by the Office of Naval Research under Grant No. N00014-90-J-1900.

REFERENCES

1. G. A. Smolensky, *J. Phy. Soc. Jpn. Suppl.* 28 (1970) 26.
2. R. Clarke and J. C. Burfoot, *Ferroelectrics* 8 (1974) 505.
3. V. J. Fritsberg, A. J. Bock and K. J. Borman, *Ferroelectrics* 8 (1974) 495.
4. W. Kanzig, *Helv. Phys. Acta.* 24 (1951) 175.
5. N. Setter and L. E. Cross, *J. Mat. Sci.* 15 (1980) 2478.
6. B. N. Rolov, *Sov. Phy. Solid State* 6 (1965) 1676.

LIST OF FIGURES

Fig. 1. A plot of dielectric constant (k) versus temperature. The value of Δ from equation (4) is also shown.

submitted for publication to J Am Ceram Soc.

Microstructure and Dielectric Characteristics of $(\text{Pb}_x\text{Ba}_{0.5-x}\text{Sr}_{0.5})\text{TiO}_3$ Ceramics.

Ramaratnam Ganesh and Edward Goo*

Department of Materials Science and Engineering, University of Southern California,
Los Angeles, California 90089.

ABSTRACT

Microstructural and dielectric properties of the $\text{Pb}_x\text{Ba}_{0.5-x}\text{Sr}_{0.5}\text{TiO}_3$ system have been studied. It is found that this system forms a perfect solid solution in the entire composition range ($0.0 \leq x \leq 0.5$) and is cubic for the $x=0, 0.1$ and 0.2 compositions and tetragonal for other compositions. Measurements of the dielectric constant as a function of temperature reveal that this materials is ferroelectric at room temperature for the $x>0.2$ compositions and has a broad paraelectric-ferroelectric transition region. No shift in the dielectric maxima was noted, however, there is a slight spread in the dielectric constant with frequency for the $x=0.4$ composition. A quantitative model to mathematically analyze the effect of composition fluctuations on the dielectric broadening for a ternary system is presented. Transmission electron microscopic studies reveals the presence of 90° ferroelectric domains oriented along the $\{01\bar{1}\}$ planes for the $x=0.3$ and 0.4 compositions.

* Member American Ceramic Society

INTRODUCTION

Ferroelectrics have become increasingly important as materials for electronic devices [1,2]. Substantial research and development has been devoted to these materials with the goal of achieving better properties. The most widely used ferroelectrics occur in the perovskite family with the general formula ABO_3 . Numerous modifications of these materials, in the form of either solid solutions or dopant additions have been researched with the aim of obtaining improved dielectric and piezoelectric properties compared to the simple perovskite. Complex perovskites with either A-site or B-site substitutions have been studied, though relatively lesser work have been done on A-site substitutions.

The dielectric and piezoelectric properties of barium titanate have been extensively studied for the past fifty years. Several modified forms of barium titanate have been used as ceramic dielectrics for high permittivity applications [3-7]. Pure barium titanate undergoes a paraelectric-ferroelectric phase transition at 120°C , which is accompanied by a sharp rise in the dielectric permittivity ($\approx 10,000$). Additions such as strontium or lead are usually employed to raise or lower the Curie point for particular applications and to maintain a fairly low temperature dependence of the dielectric constant.

Barium titanate and strontium titanate are known to form solid solutions with each other at all compositions because of their identical crystal structure and comparable ionic radii of Ba^{2+} and Sr^{2+} ions [8-9]. Variation of strontium titanate composition offers good control over many of the desired dielectric characteristics and therefore, has been extensively studied [10-12]. $\text{Ba}_x\text{Sr}_{1-x}\text{TiO}_3$ is ferroelectric at room temperature for the barium rich compositions and has a Curie temperature of -37°C for the $x=0.5$ composition. It has been the object of extensive research to find some composition where the dielectric peak would

spread out with a reasonably constant high value over the working temperature range. Since, these materials find potential application in devices where the working range is close to room temperature any additions that would increase the dielectric constant at room temperature and increase the diffuseness of the paraelectric-ferroelectric phase transition would be desirable. Lead titanate has a tetragonal crystal structure with a fairly high c/a ratio of 1.06 and is ferroelectric at room temperature. The transition to the ferroelectric tetragonal phase from the cubic paraelectric phase occurs at 490°C . Therefore, addition of PbTiO_3 to $\text{Ba}_{0.5}\text{Sr}_{0.5}\text{TiO}_3$ would increase the dielectric constant at room temperature and at the same time increase the width of the paraelectric-ferroelectric transition region as statistically greater fluctuations in composition is possible. No prior work has been done in the $(\text{Pb},\text{Ba},\text{Sr})\text{TiO}_3$ ternary system and, therefore, it is of considerable scientific and technological interest to examine its dielectric and microstructural behavior.

The present work aims to study the microstructure through X-ray diffraction and transmission electron microscopy investigations in the $\text{Pb}_x\text{Ba}_{0.5-x}\text{Sr}_{0.5}\text{TiO}_3$ system and examine its dielectric properties. Ferroelectrics with diffuse phase transitions have been reported as early as the 1950s. In this paper we present our observations on the effect of variations in composition on the diffuse phase transitions and microstructure in the $\text{Pb}_x\text{Ba}_{0.5-x}\text{Sr}_{0.5}\text{TiO}_3$ system. A theoretical model to quantitatively estimate the size of the Koznjg regions for a ternary system is also presented.

EXPERIMENTAL PROCEDURE

Conventional powder processing techniques were employed to prepare the bulk powders. Stoichiometric amounts of the chemically pure lead oxide (99.5%), barium carbonate

(99.6%), strontium carbonate (99.5%) and titanium dioxide (99.7%) were weighed and then ball milled for five hours in deionized water, followed by oven drying of the filtrate residue. The ceramic powders were calcined at 850°C for five to eight hours in a covered alumina crucible. The calcined residue was ball milled again and the final product was ground using a mortar and pestle into a fine powder. The calcined powders were then cold pressed in a hydraulic press at 35,000 psi into cylindrical pellets with 25mm diameter and 3mm thickness. The compacts were then sintered at 1300°C for five hours in a covered alumina crucible loosely packed with powder of the same composition to minimize the loss of lead due to vaporization. Samples of $\text{Pb}_x\text{Ba}_{0.5-x}\text{Sr}_{0.5}\text{TiO}_3$ were prepared in the composition range 0-0.5 in increments of 0.1.

For X-ray diffraction studies a mechanically polished sintered specimen was used. X-ray studies were done on a Rigaku diffractometer operating at 35kV and 50mA. TEM samples were prepared by cutting 3mm diameter circular disks using an ultrasonic drill. The disks were mechanically polished and dimpled to 20 micron thickness, mounted on a copper grid and milled using a beam of argon ions. TEM studies were done on a Philips EM 420 machine operating at an accelerating voltage of 120kV. High resolution TEM studies were done on a Akashi 002B microscope operating at 200kV. Dielectric measurements were done using a Keithley 3322 LCZ meter. Silver electrodes were evaporated on the samples with a Denton vacuum evaporator. Grain size measurements were done on a Cambridge SEM operating at 20kV.

X-RAY AND GRAIN SIZE MEASUREMENTS

X-ray studies done on this system reveal that the material is cubic for $x=0, 0.1$ and 0.2 compositions and tetragonal for other compositions. The results are shown in Table-1.

For the $x=0$ and 0.1 compositions additional $K\alpha_2$ peaks were seen at higher angles. The x-ray scan for the $\text{Pb}_{0.1}\text{Ba}_{0.4}\text{Sr}_{0.5}\text{TiO}_3$ composition is shown in Figure 1. Co-existence of a ferroelectric tetragonal phase and a paraelectric cubic phase have been reported for the $x=0.76$ and 0.715 compositions in the $\text{Ba}_x\text{Sr}_{1-x}\text{TiO}_3$ system [10]. This is believed to be due to the preferential diffusion of Sr^{2+} ions into BaTiO_3 . In order to check if a similar behavior exists in the present system the (200) reflections from the x-ray scan were analyzed. In the event of co-existing phases, these reflections would consist of a doublet corresponding to the tetragonal symmetry and a singlet corresponding to the cubic symmetry. The line intensities are strong enough to allow any appreciable differences to be observed. Our analysis did not reveal the co-existence of two or more phases for any given composition. However, segregation of an amorphous phase or a secondary phase not readily observable in x-ray scans is not uncommon [13]. High resolution TEM studies were done to check for the presence of any grain boundary phase. Fig. 2. shows the high resolution TEM picture of a typical grain boundary region for the $x=0.3$ composition. The grain boundaries are devoid of any secondary phases. Similar microstructure was noted for other compositions as well. Therefore, it is concluded that $\text{Pb}_x\text{Ba}_{0.5-x}\text{Sr}_{0.5}\text{TiO}_3$ forms a perfect solid solution in the entire composition range.

The grain size was measured using the circular intercept method specified by ASTM Standard E112 [14]. Fig. 3. shows the grain size and morphology for the $\text{Pb}_{0.3}\text{Ba}_{0.2}\text{Sr}_{0.5}\text{TiO}_3$ sample. The grain size for different compositions studied is given in Table 1. No specific trend is noticed in the grain size with change in composition.

DIELECTRIC STUDIES

The dielectric constant (k) as a function of temperature was measured for various compositions in the $\text{Pb}_x\text{Ba}_{0.5-x}\text{Sr}_{0.5}\text{TiO}_3$ ternary system and is shown in Fig. 4. A plot of the dielectric constant curves at different frequencies for the $x=0.3$ and 0.4 compositions are shown in Fig. 5. No shift is observed in the maxima of the dielectric curves at different frequencies indicating the absence of relaxor behavior in this system. However, for the $x=0.4$ composition it is seen that above the Curie point there is a spread in the k values at different frequencies. This is unusual because, ideally at frequencies below 10^7 hz. the total polarizability is a sum of the ionic, electronic and dipolar polarizabilities and all of them are active within the frequency range studied. Therefore, the k values should have nearly identical values at different frequencies unlike that observed for the $x=0.4$ composition. The exact reason for this type of behavior is still unknown. However, a possible reason could be the increase in the internal stress due to the increase in the c/a ratio as the lead content increases, thereby, resulting in a spread in the k values at different frequencies.

The Curie point increases with increasing additions of lead as shown in Fig. 6 and the dielectric maxima decreases as the lead content increases. This expected as PbTiO_3 has a higher Curie point and a lower dielectric maxima as compared to BaTiO_3 . For the $x=0.2$ composition the paraelectric-ferroelectric transition occurs at 14.5°C and has a room temperature dielectric constant of approximately 5000. For the $x>0.2$ compositions the material is ferroelectric at room temperature.

The dielectric constant, k , as a function of temperature can be written as [15]

$$\frac{1}{k} = \frac{1}{k_{\max}} \left[1 + \frac{(T-T_c)^{\gamma}}{\delta} \right] \quad (1)$$

where k_{\max} is the maximum in the dielectric constant, T_c is the Curie temperature and δ is the diffuseness parameter. γ is an empirical term having a value of one for ideal Curie-Weiss behavior and a value of two for relaxor behavior [15]. For other materials γ generally lies between these two values. A plot of γ and δ as a function of composition for the $\text{Pb}_x\text{Ba}_{0.5-x}\text{Sr}_{0.5}\text{TiO}_3$ system is shown in Fig. 7. It is seen that except for the 0.1 composition, both γ and δ increase with increasing lead content. The exact reason for the higher γ value for the 0.1 composition is not clear.

The diffuseness behavior in solid solutions is primarily attributed to compositional fluctuations in a microscopic scale [16-17]. Each of these microregions, also known as Kanzig regions [18], have different composition and hence, different Curie temperatures for the onset of ferroelectricity. If such statistical fluctuations in composition are responsible for the spread in the transition region then the maximum diffuseness should occur at the $x=0.25$ composition unlike that observed in the present system. However, with increasing additions of PbTiO_3 the c/a ratio increases and therefore, the internal stress becomes greater as the crystal is cooled through the Curie point. For materials under stress there is a broadening of the paraelectric-ferroelectric transition region [19]. This explains the increase in the width of the transition region with increasing lead content in the $\text{Pb}_x\text{Ba}_{0.5-x}\text{Sr}_{0.5}\text{TiO}_3$ system.

A mathematical treatment on the effect of compositional fluctuations on the diffuseness of the paraelectric-ferroelectric phase transition for a solid solution of two compounds with perovskite structure was reported by Smolensky [16]. Attempts to extrapolate these results to different binary systems have been made, however, no report exists on analyzing the diffuseness behavior for the ternary systems. In this paper we present a theoretical model to analyze the effect of compositional fluctuations on the width of the

transition region for the $\text{Pb}_x\text{Ba}_{0.5-x}\text{Sr}_{0.5}\text{TiO}_3$ system.

Consider a ternary system of the type $\text{A}_x\text{B}_y\text{C}_{1-x-y}\text{TiO}_3$. The macroscopic compositions of A, B and C are therefore, x, y and 1-x-y respectively. In a microvolume containing a total of N molecules of $(\text{A,B,C})\text{TiO}_3$, the probability, $P(m,n)$, of finding m molecules of ATiO_3 and n molecules of BTiO_3 is given by,

$$P(m,n) = \frac{N!}{m!n!(N-m-n)!} x^m y^n (1-x-y)^{(N-m-n)} \quad (2)$$

Where $N! = N(N-1)(N-2) \dots 3.2.1$. Using Stirling's approximation for large N we have

$$N! = \sqrt{2\pi N} \left(\frac{N}{e}\right)^N \quad (3)$$

Using this approximation in the earlier equation we have

$$P(m,n) = \frac{\sqrt{N} (N)^N x^m y^n (1-x-y)^{(N-m-n)}}{2\pi \sqrt{nm(N-m-n)} n^m m^n (N-m-n)^{(N-m-n)}} \quad (4)$$

If $\alpha = m/N$ and $\beta = n/N$ represent the composition of the microvolume we have

$$P(m,n) = \frac{x^{N\alpha} y^{N\beta} (1-x-y)^{N(1-\alpha-\beta)}}{2\pi N \sqrt{\alpha\beta(1-\alpha-\beta)} \alpha^{N\alpha} \beta^{N\beta} (1-\alpha-\beta)^{N(1-\alpha-\beta)}} \quad (5)$$

If $\alpha - x = \delta_1$ and $\beta - y = \delta_2$, then δ_1 and δ_2 represent the deviations of the microscopic composition from the macroscopic composition. For a given N we can plot $P(m,n)$ as

function of these deviations to identify how the diffuseness varies with fluctuations in composition for a ternary system. Plots of $P(m,n)$ as a function of δ_1 and δ_2 for a given N for the $A_xB_{0.5-x}C_{0.5}TiO_3$ system are shown in Fig. 8. It is seen that the diffuseness is maximum for the $x=0.25$ composition and the curves are symmetric about $\delta_{1,2}=0$. These plots are similar to plots obtained for the binary systems [16]. In order to correlate the diffuseness seen in $P(m,n)$ with the diffuseness of the dielectric curves it is necessary to obtain the width at half maximum (WHM) from the above equations. It is clearly seen from Fig. 8. that $P(m,n)$ is maximum when both δ_1 and δ_2 are zero. Therefore, substituting $\alpha=x$ and $\beta=y$ in equation-5 we have

$$P(m,n) = \frac{1}{2\pi N\sqrt{\alpha\beta(1-\alpha-\beta)}} \quad (6)$$

Therefore the value at half maximum is given by

$$\frac{P_{\max}(m,n)}{2} = \frac{1}{4\pi N\sqrt{\alpha\beta(1-\alpha-\beta)}} \quad (7)$$

Substituting this in equation-5 we have

$$\frac{x^{N\alpha}y^{N\beta}(1-x-y)^{N(1-\alpha-\beta)}}{\alpha^{N\alpha}\beta^{N\beta}(1-\alpha-\beta)^{N(1-\alpha-\beta)}} = \frac{1}{2}$$

For small fluctuations in composition we assume that the Curie point varies linearly with composition. Therefore, for a δx or a δy change in composition, the macroscopic Curie

temperature, T_c of the ternary $A_xB_yC_{1-x-y}TiO_3$ is given by $T_c = T_ax + T_by + T_c(1-x-y)$, where, T_a , T_b and T_c are the Curie temperatures of $ATiO_3$, $BTiO_3$ and $CTiO_3$ respectively. The gradient of T_c (∇T_c) is given by

$$\nabla T_c = \frac{\partial T_c}{\partial x} \vec{i} + \frac{\partial T_c}{\partial y} \vec{j} \quad (9)$$

where \vec{i} and \vec{j} are the unit vectors along the x and y directions respectively. Mathematically, $\partial T_c / \partial x$ and $\partial T_c / \partial y$ represent the change in the value of T_c as we change x and y respectively by small amounts. If we have $\alpha - x = f(T - T_c)$ and $\beta - y = g(T - T_c)$, where f and g are proportionality constants, then $1/f = \partial T_c / \partial x$ and $1/g = \partial T_c / \partial y$. If $T - T_c = \Delta$ then, $\alpha - x = \Delta / (\partial T_c / \partial x)$ and $\beta - y = \Delta / (\partial T_c / \partial y)$. If we substitute these values in equation-8 then, Δ represents the width at half maximum with respect to T and is experimentally obtained from the dielectric constant versus temperature curves. Using the experimentally calculated value of Δ in equation-8, we can obtain the value of N and hence, the size of the Kanzig regions. Using T_a , T_b and T_c as $490^\circ C$, $120^\circ C$ and $-265^\circ C$ respectively and a cell volume of 64 \AA^3 , the size of the Kanzig regions for the $Pb_xBa_{0.5-x}Sr_{0.5}TiO_3$ system was estimated to lie in the range of $15-30 \text{ \AA}$. It should be noted that the above treatment does not include the effect of internal stress on the spread of the transition region.

TEM STUDIES

Selected area electron diffraction patterns from the three principal zone axes for the $Pb_xBa_{0.5-x}Sr_{0.5}TiO_3$ system are shown in Fig. 9. Electron diffraction studies did not reveal the presence of any secondary phases confirming that $Pb_xBa_{0.5-x}Sr_{0.5}TiO_3$ forms a complete solid

solution in the composition range studied. Presence of transformation domains was evidenced for the $x=0.3, 0.4$ and 0.5 compositions as shown in Fig. 10. These are 90° ferroelectric domains where the direction of the polar axis remains unchanged within each domain but is rotated 90° from domain to domain. The polarization vector assumes a "head-tail" arrangement to maintain charge neutrality at the domain wall. A schematic of the domain wall arrangement is shown in Fig. 11. The transformation domains are formed when the cubic paraelectric phase transforms to the tetragonal ferroelectric phase. The domain boundaries are planar and lie on well defined crystallographic planes. In the $\text{Pb}_x\text{Ba}_{0.5-x}\text{Sr}_{0.5}\text{TiO}_3$ system the domain boundaries lie along the $(01\bar{1})$ planes. Electron diffraction patterns from a region consisting of 90° domains for the $x=0.3$ composition is shown in Fig. 12. No spot splitting was seen even for higher index planes. In the case of $\text{Pb}_{0.3}\text{Ba}_{0.2}\text{Sr}_{0.5}\text{TiO}_3$ the c/a ratio is 1.005 and therefore, it is difficult to see the effect of 90° rotation in the diffraction patterns. High resolution TEM studies were done to observe if any difference in the arrangement of the atoms were visible across the domain boundaries. No perceptible difference in the arrangement of the atoms was noticed as shown in Fig. 13. even though the 90° domains were visible at low magnifications. This is not unusual as there is only a 0.5% difference between the a and c values making it difficult to observe the change in the high resolution image or observe the spot splitting in the diffraction patterns. The effect of the c/a ratio on the atom positions across the twin domain is shown in Fig. 11. No 180° domains were observed in any of the compositions studied.

CONCLUSIONS

Microstructure and dielectric studies in the $\text{Pb}_x\text{Ba}_{0.5-x}\text{Sr}_{0.5}\text{TiO}_3$ system are reported. Studies reveal that $\text{Pb}_x\text{Ba}_{0.5-x}\text{Sr}_{0.5}\text{TiO}_3$ forms a perfect solid solution in the entire composition

range and is cubic for the $x=0$, 0.1 and 0.2 composition and tetragonal for the other compositions studied. The c/a ratio increases with increasing lead content. Dielectric studies reveal that this system is ferroelectric for the $x>0.2$ compositions and has a broad paraelectric-ferroelectric transition region. No shift in the dielectric maxima with frequency was observed. However, a spread in the k values as function of frequency was observed for the $\text{Pb}_{0.4}\text{Ba}_{0.1}\text{Sr}_{0.5}\text{TiO}_3$ composition. A mathematical model to quantitatively estimate the size of the Kanzig regions for a ternary system is reported and the size of the Kanzig regions for the present system was found to lie in the range of 15-30Å. TEM studies revealed the presence of transformation twins lying along the $(01\bar{1})$ planes for the 0.3, 0.4 and 0.5 compositions. No 180° ferroelectric domains were observed although 90° domains were clearly seen for the 0.3, 0.4 and 0.5 compositions.

ACKNOWLEDGEMENT

The authors would like to acknowledge the use of Philips 420 and the Akashi 002B electron microscope and the use of the Rigaku X-ray diffractometer at the Center for Electron Microscopy and Microanalysis (CEMMA) at USC. This work was supported by the Office of Naval Research under Grant No. N00014-90-J-1900.

REFERENCES

1. R. E. Newnham and G. R. Rushan, "Smart Electronics," *J. Am. Cer. Soc.*, **74**, 463-479 (1991).
2. R. E. Newnham, "The Golden Age of Electronics," *Adv. Cer. Matl.*, **3**, 12-16 (1988).

3. V. C. Sanvordenker, "Optical and Microstructural Variations with Electric Field in Barium-Strontium Titanate Ceramics," *J. Am. Cer. Soc.*, **50**, 261-265 (1967).
4. T. Nomura and T. Yamaguchi, "TiO₂ Aggregation and Sintering of BaTiO₃ Ceramics," *Am. Cer. Soc. Bull.*, **59**, 453-55 (1980).
5. W. Y. Howng and C. McCutcheon, "Electrical Properties of Semiconducting BaTiO₃ by Liquid Phase Sintering," *Am. Cer. Soc. Bull.*, **62**, 231-34 (1983).
6. N. M. Molokhia, M. A. Issa and N. A. Nasser, "Dielectric and X-ray Diffraction Studies of BaTiO₃ Doped with Ytterbium," *J. Am. Cer. Soc.*, **67**, 289-91 (1984).
7. U. Syamaprasad, R. K. Galgali and B. C. Mohanty, "A modified Barium Titanate for Capacitors," *J. Am. Cer. Soc.*, **70**, C147-C148 (1987).
8. D. Kolar, M. Trotelj and Z. Stadler, "Influence of Interdiffusion on Solid Solution Formation of Sintering in the System BaTiO₃-SrTiO₃," *J. Am. Cer. Soc.*, **65**, 470-474 (1982).
9. A. Basmajian and R. S. de Vries, "Phase Equilibria in the System BaTiO₃-SrTiO₃," *J. Am. Cer. Soc.*, **40**, 373 (1957).
10. D. Barb, E. Barbulescu and A. Barbulescu, "Diffuse Phase Transitions and Ferroelectric-Paraelectric Diagram for BaTiO₃-SrTiO₃ system," *Phys. Stat. Solidi A*, **74**, 79-83 (1982).
11. E. N. Bunting, G. R. Shelton and A. S. Creamer, "Properties of Barium-Strontium Titanate Dielectrics," *J. Res. Natl. Bur. Std.*, **38**, 337-49 (1947).
12. L. Benguigui and K. Bethe, "Diffused Phase Transitions in Ba_xSr_{1-x}TiO₃ Single Crystals," *J. App. Phy.*, **47**, 2787-91 (1976).
13. D. R. Clarke and G. Thomas, "Grain Boundary Phases in a Hot-Pressed MgO Fluxed Silicon Nitride," *J. Am. Cer. Soc.*, **60** 491-95 (1977).

14. 1985 Annual Book of ASTM Standards, *ASTM*, 117-149 (1985).
15. K. Uchino and S. Nomura, "Critical Exponents of the Dielectric Constants in Doped-Phase-Transition Crystals," *Ferroelect. Lett.*, **44**, 55-61 (1982).
16. G. A. Smolensky, "Physical Phenomena in Ferroelectric with Diffused Phase transitions," *J. Phy. Soc. Jpn.*, **28** (Suppl.), 26-37 (1970).
17. B. N. Rolov, "Effect of Composition Fluctuations on Unsharp Ferroelectric Phase Transitions," *Sov. Phy-Solid-State*, **6**, 1676-1678 (1965).
18. W. Kanzig, "X-ray Investigations in Barium Titanate Ferroelectricity," *Helv. Phys. Acta*, **24**, 175-216 (1951).
19. N. Setter and L. E. Cross, "Pressure Dependence of the Dielectric Properties of $\text{Pb}(\text{Sc}_{1/2}\text{Ta}_{1/2})\text{O}_3$," *Phy. Stat. Solidi*, **61**, K71-K75 (1980).

List of Figures

- Fig. 1. XRD patterns for the $\text{Pb}_{0.1}\text{Ba}_{0.4}\text{Sr}_{0.5}\text{TiO}_3$ composition.
- Fig. 2a) High resolution electron micrograph of a typical grain boundary region for the $x=0.3$ composition. 2b) The grain boundary at a lower magnification.
- Fig. 3. SEM micrograph showing the grain size and morphology for the $\text{Pb}_{0.3}\text{Ba}_{0.2}\text{Sr}_{0.5}\text{TiO}_3$ composition.
- Fig. 4. Dielectric constant as a function of temperature at 100kHz for a) $x=0.0$ b) $x=0.1$ c) $x=0.2$ d) $x=0.3$ and e) $x=0.4$ in the $\text{Pb}_x\text{Ba}_{0.5-x}\text{Sr}_{0.5}\text{TiO}_3$ system.
- Fig. 5. Dielectric constant at different frequencies for a) $\text{Pb}_{0.3}\text{Ba}_{0.2}\text{Sr}_{0.5}\text{TiO}_3$ composition and b) $\text{Pb}_{0.4}\text{Ba}_{0.1}\text{Sr}_{0.5}\text{TiO}_3$ composition.
- Fig. 6. Curie point (T_c) as a function of composition for $\text{Pb}_x\text{Ba}_{0.5-x}\text{Sr}_{0.5}\text{TiO}_3$ system.
- Fig. 7. Variation of a) γ and b) δ as a function of composition for the $\text{Pb}_x\text{Ba}_{0.5-x}\text{Sr}_{0.5}\text{TiO}_3$ system.
- Fig. 8. $P(m,n)$ as a function of δ_1 and δ_2 for a) $x=0.1, 0.4$ b) $x=0.2, 0.3$ and c) $x=0.25$ in the $\text{A}_x\text{B}_{0.5-x}\text{C}_{0.5}\text{TiO}_3$ system. A value of 500 was used for N for each of these plots.
- Fig. 9. Electron diffraction patterns from a) $[111]$ b) $[110]$ and c) $[100]$ zone axes for the $\text{Pb}_x\text{Ba}_{0.5-x}\text{Sr}_{0.5}\text{TiO}_3$ system.
- Fig. 10. Bright field image showing the presence of ferroelectric domains along the $(01\bar{1})$ planes for the $x=0.3$ composition.
- Fig. 11. A schematic diagram of the domain wall arrangement for a) 10% difference in the c and a values and b) less than 0.5% difference in the c and a values.

Fig. 12. Electron diffraction pattern from the [111] zone axes showing the absence of spot splitting.

Fig. 13. High resolution electron micrograph showing no perceptible variation in lattice spacing across the domain boundary. The approximate position of the domain boundary is indicated by the arrows marked d.

Table 1. Lattice parameters, crystal structure and grain size for the $\text{Pb}_x\text{Ba}_{0.5-x}\text{Sr}_{0.5}\text{TiO}_3$ system.

X	Lattice Parameter (Å)	Crystal Structure	Grain Size (μm)
0.0	a=3.947	Cubic	4.17
0.1	a=3.951	Cubic	4.3
0.2	a=3.952	Cubic	4.27
0.3	a=3.941 c=3.950	Tetragonal	4.32
0.4	a=3.932 c=3.953	Tetragonal	4.21
0.5	a=3.896 c=3.961	Tetragonal	4.25

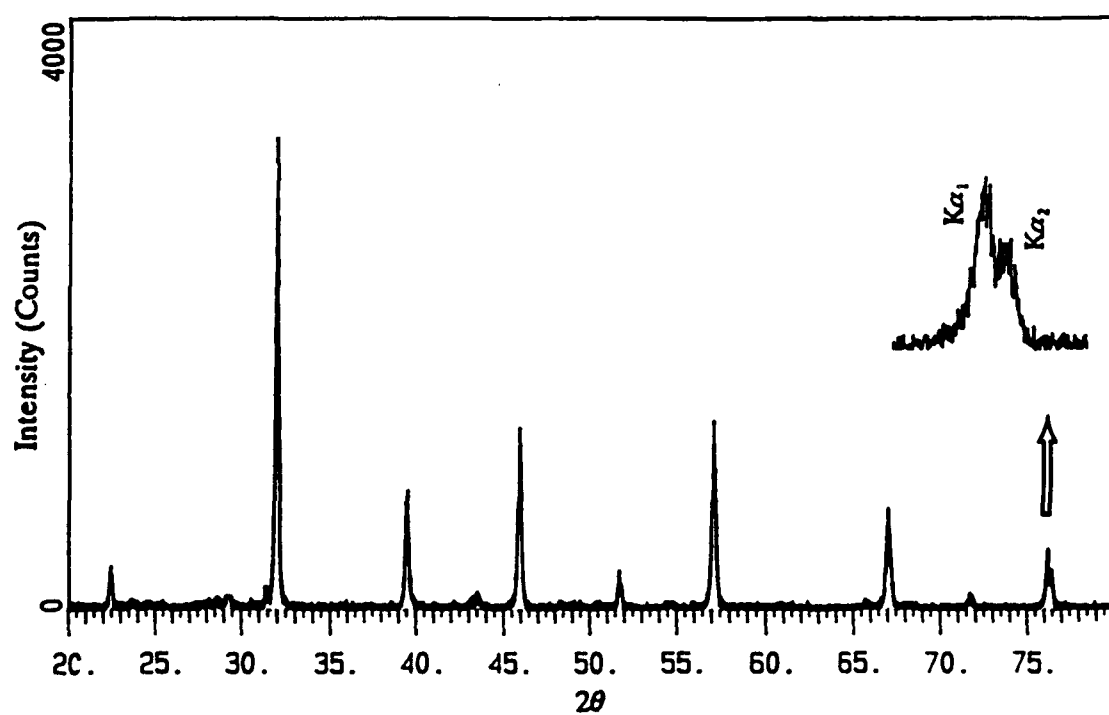


Fig. 1. XRD patterns for the $\text{Pb}_{0.1}\text{Ba}_{0.4}\text{Sr}_{0.5}\text{TiO}_3$ composition.

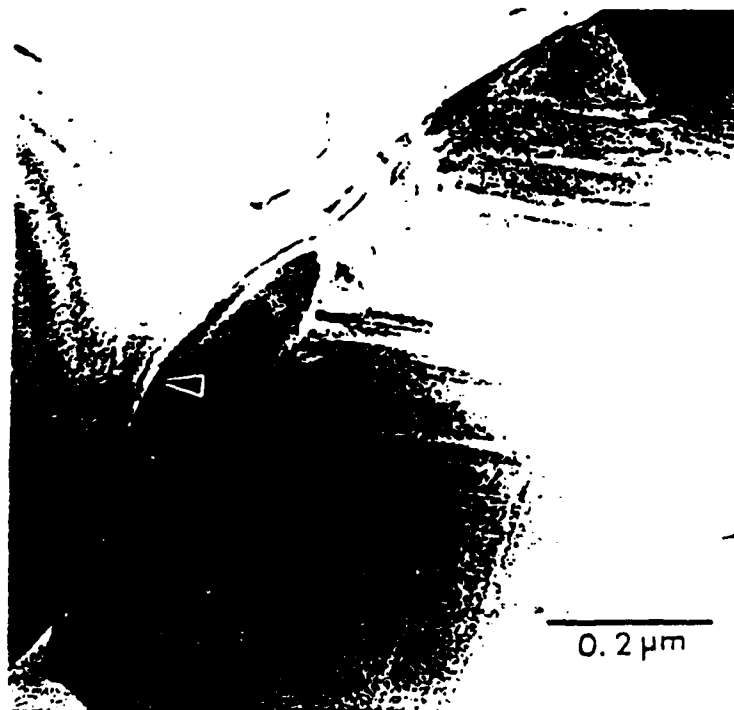
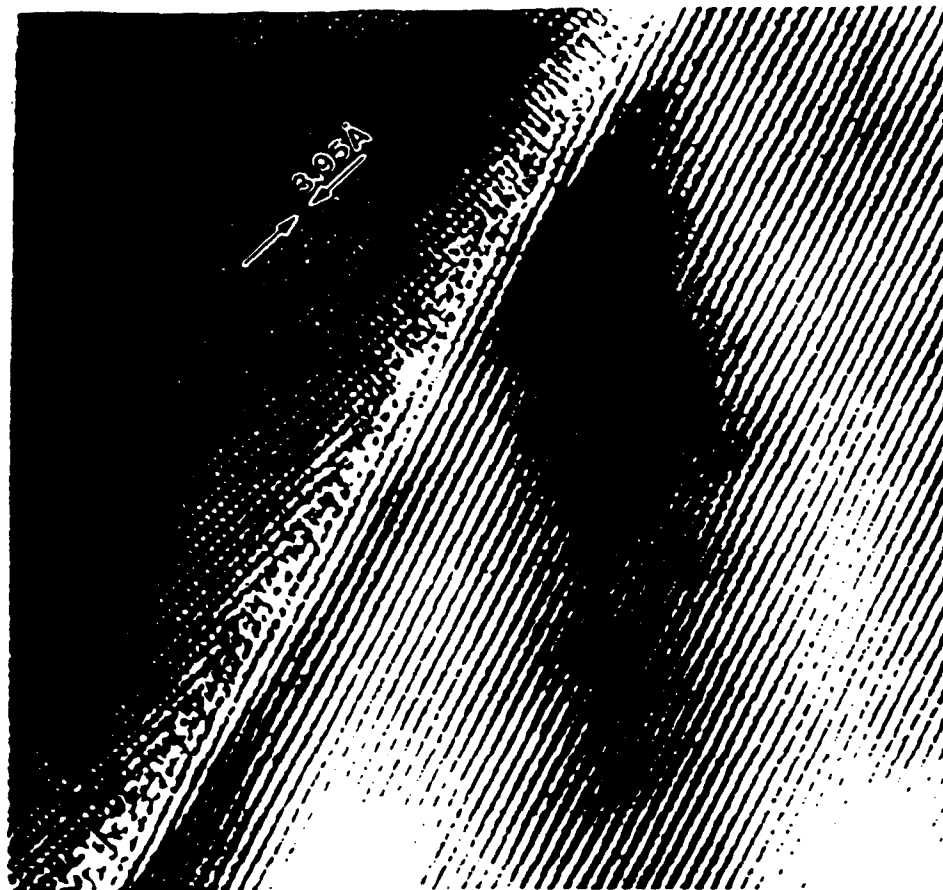


Fig. 2a) High resolution electron micrograph of a typical grain boundary region for the $x=0.3$ composition. 2b) The grain boundary at a lower magnification.

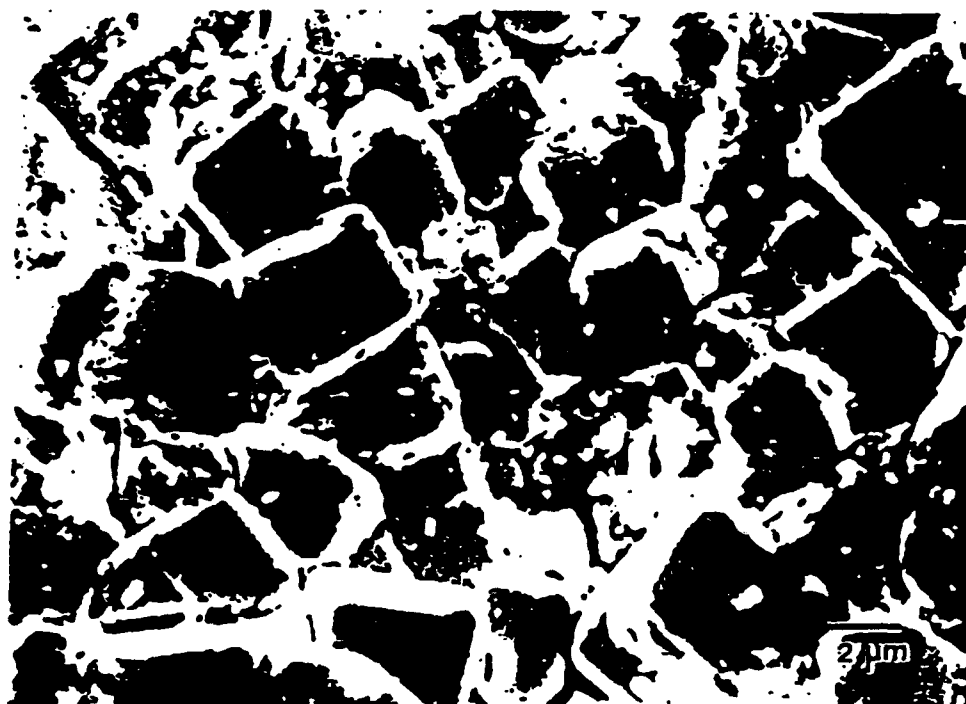


Fig. 3. SEM micrograph showing the grain size and morphology for the $\text{Pb}_{0.3}\text{Ba}_{0.2}\text{Sr}_{0.5}\text{TiO}_3$ composition.

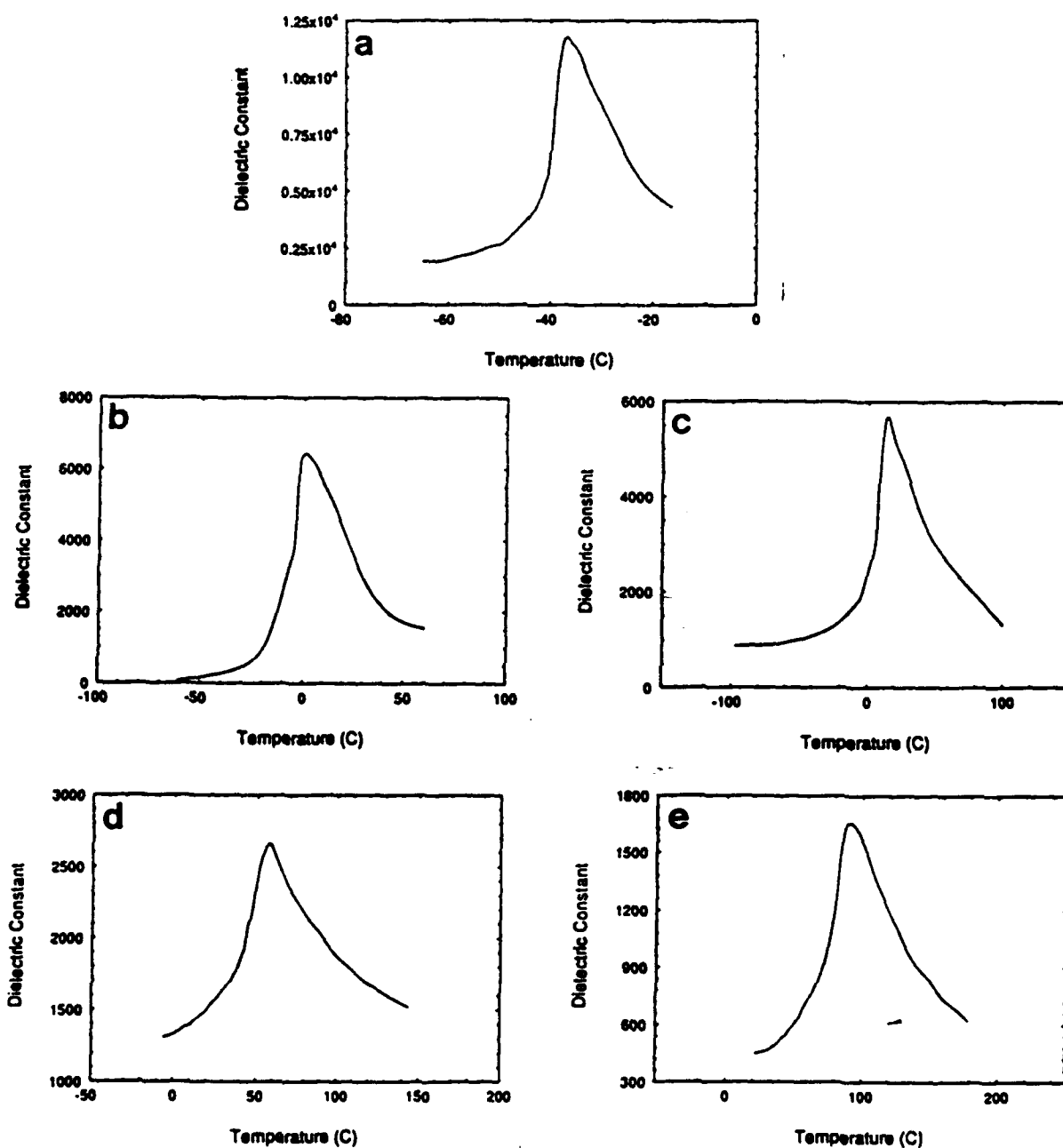


Fig. 4. Dielectric constant as a function of temperature at 100kHz for a) $x=0.0$ b) $x=0.1$ c) $x=0.2$ d) $x=0.3$ and e) $x=0.4$ in the $\text{Pb}_x\text{Ba}_{0.5-x}\text{Sr}_{0.5}\text{TiO}_3$ system.

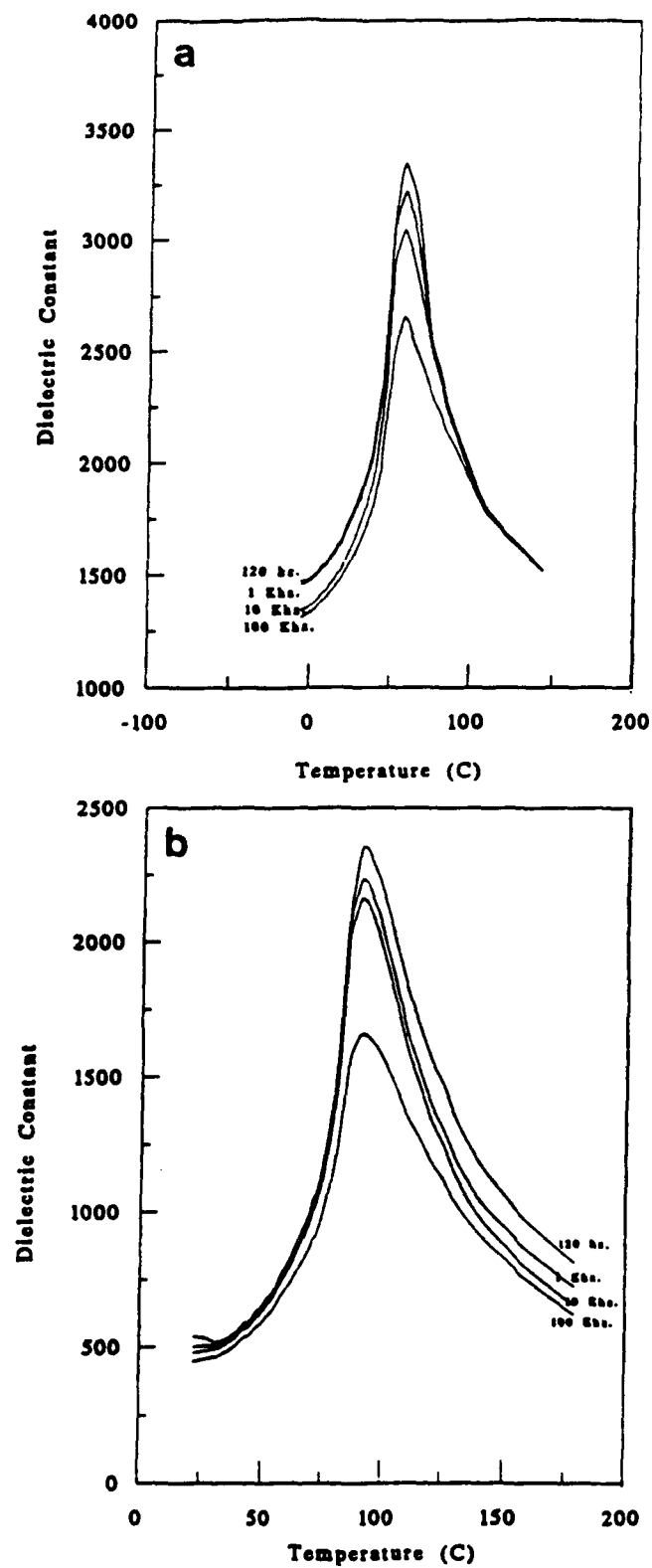


Fig. 5. Dielectric constant at different frequencies for a) $\text{Pb}_{0.3}\text{Ba}_{0.2}\text{Sr}_{0.5}\text{TiO}_3$ composition and b) $\text{Pb}_{0.4}\text{Ba}_{0.1}\text{Sr}_{0.5}\text{TiO}_3$ composition.

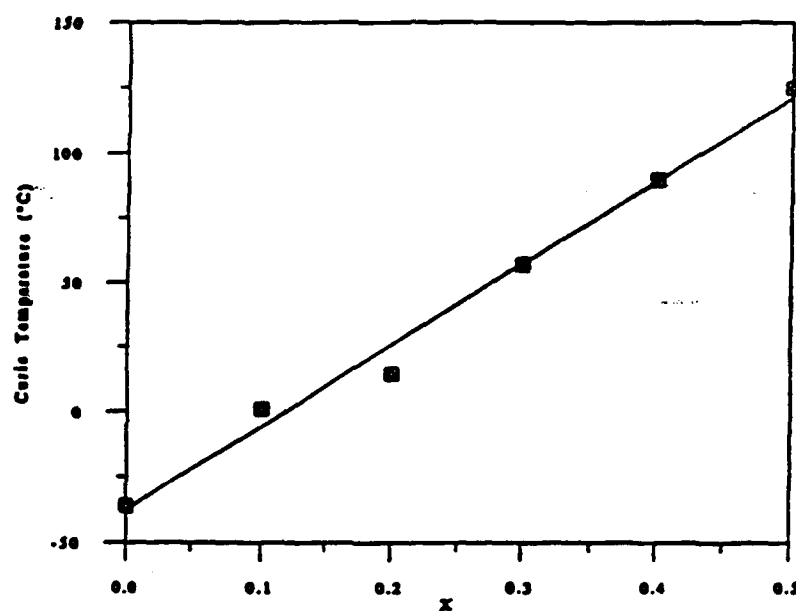


Fig. 6. Curie point (T_c) as a function of composition for the $\text{Pb}_x\text{Ba}_{0.5-x}\text{Sr}_{0.5}\text{TiO}_3$ system.

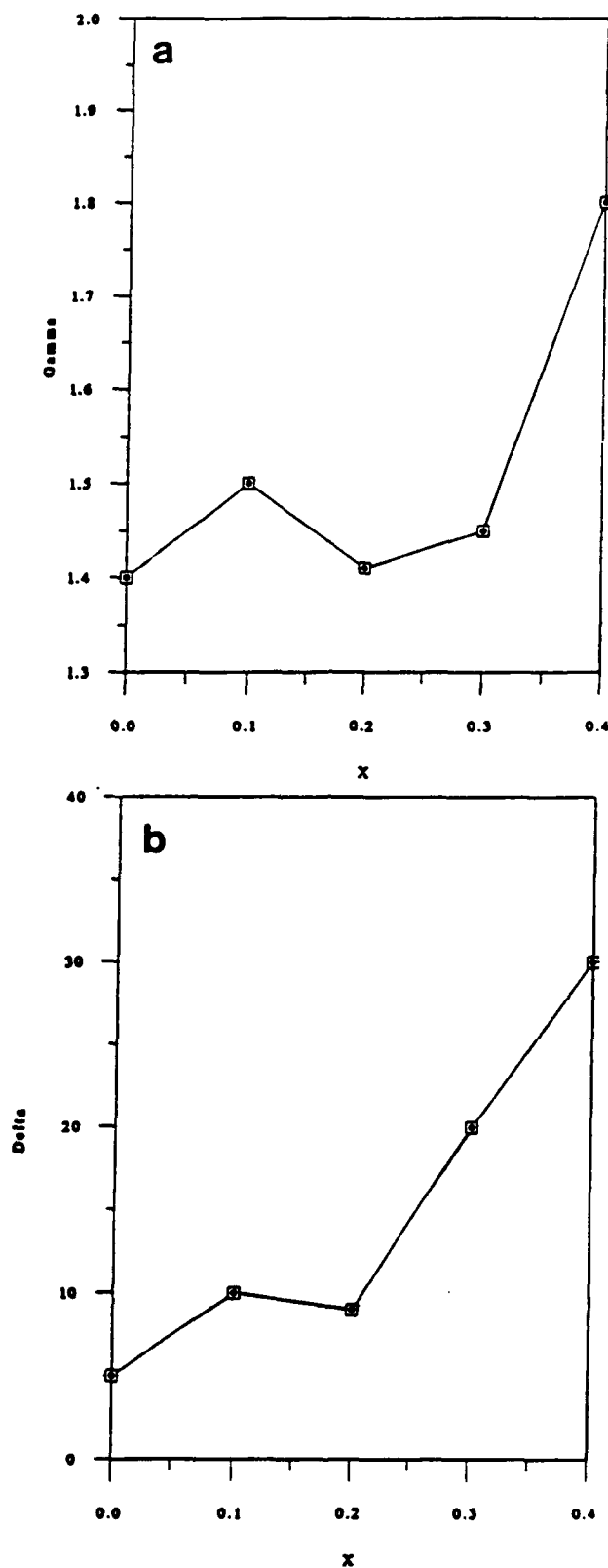


Fig. 7. Variation of a) γ and b) δ as a function of composition for the $\text{Pb}_x\text{Ba}_{0.5-x}\text{Sr}_{0.5}\text{TiO}_3$ system.

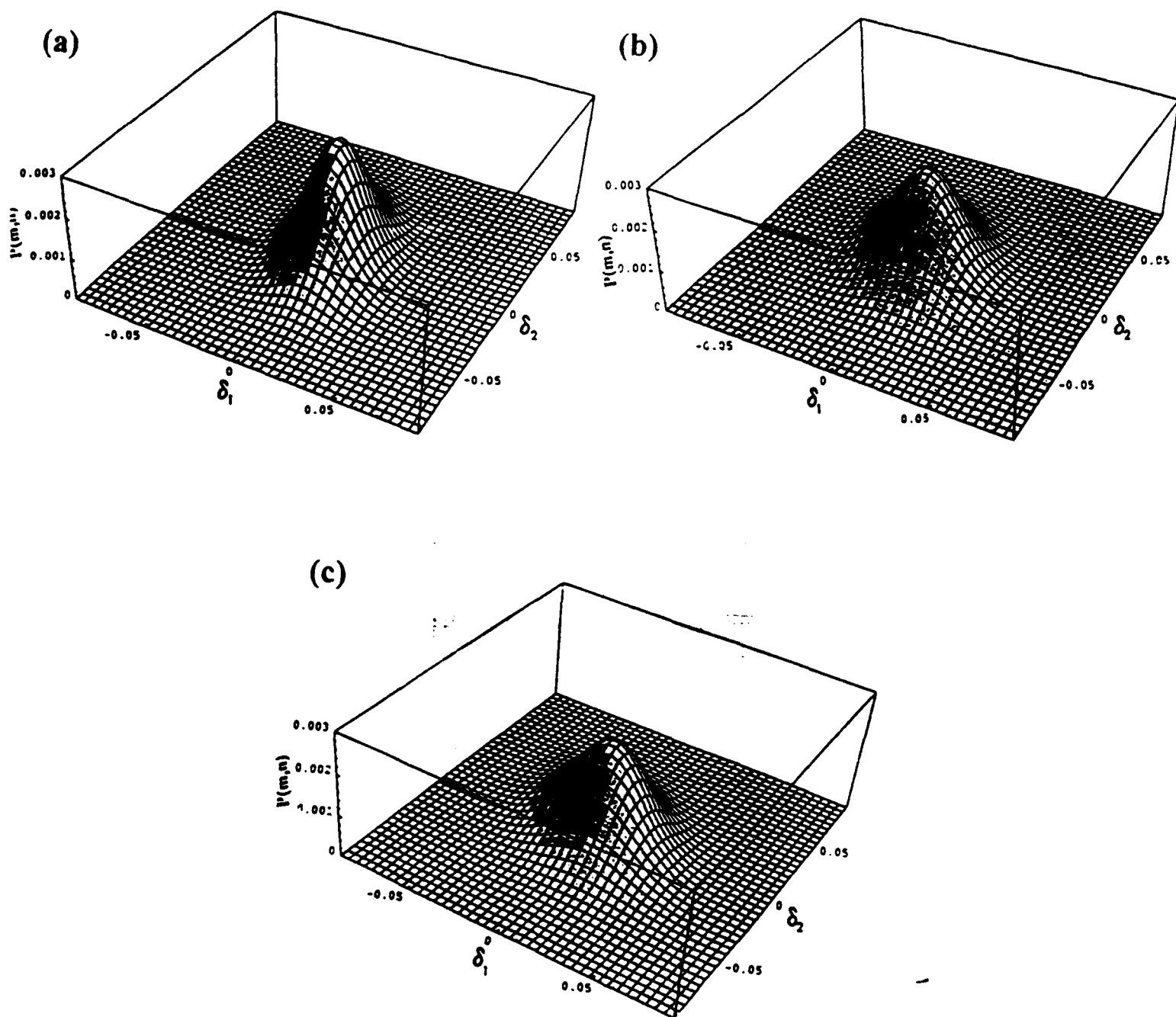


Fig. 8. $P(m,n)$ as a function of δ_1 and δ_2 for a) $x=0.1, 0.4$ b) $x=0.2, 0.3$ and c) $x=0.25$ in the $A_xB_{0.5-x}C_{0.5}TiO_3$ system. A value of 500 was used for N for each of these plots.

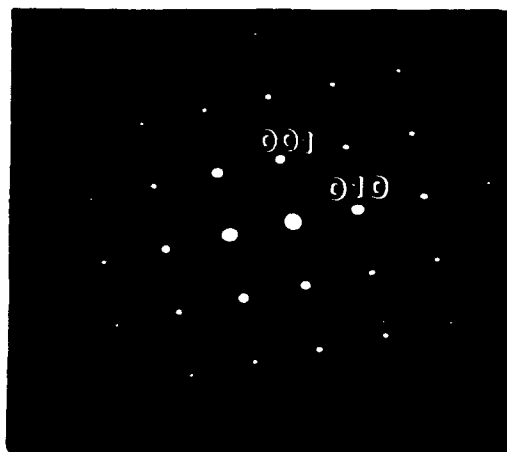
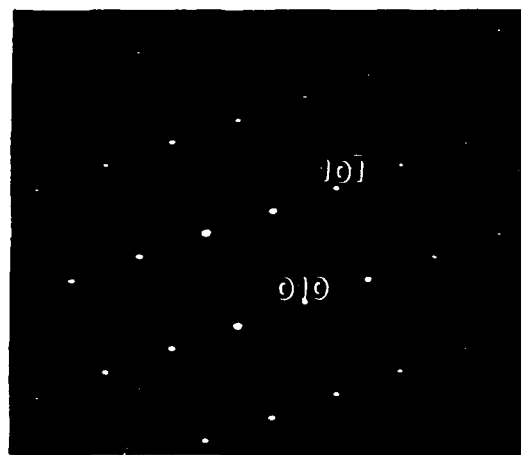
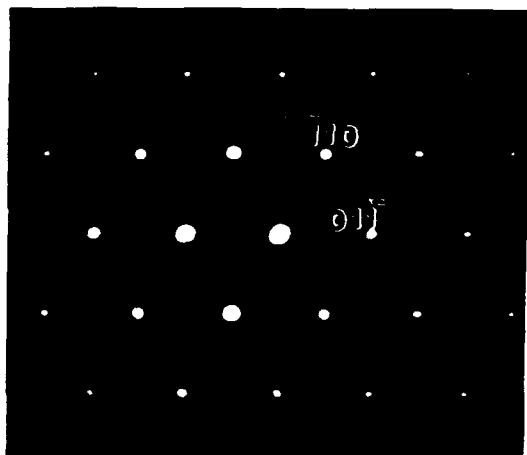


Fig. 9. Electron diffraction patterns from a) [111] b) [110] and c) [100] zone axes for the $\text{Pb}_x\text{Ba}_{0.5-x}\text{Sr}_{0.5}\text{TiO}_3$ system.



Fig. 10. Bright field image showing the presence of ferroelectric domains along the $(01\bar{1})$ planes for the $x=0.3$ composition.

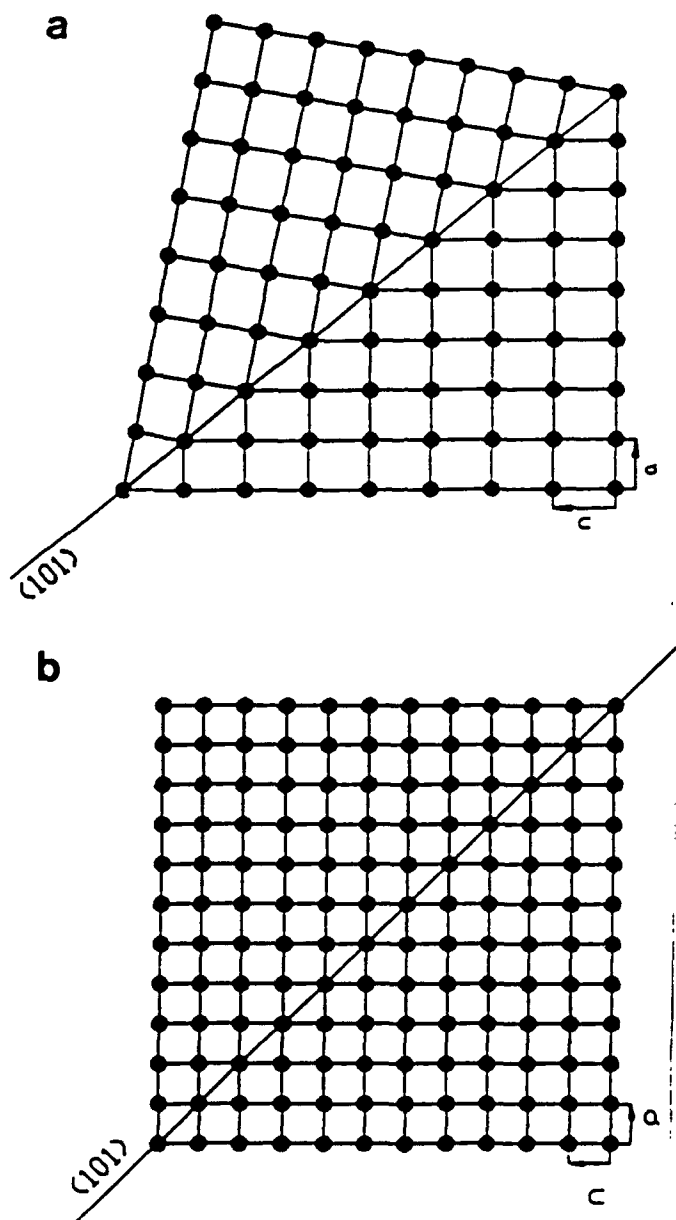


Fig. 11. A schematic diagram of the domain wall arrangement for a) 10% difference in the c and a values and b) less than 0.5% difference in the c and a values.

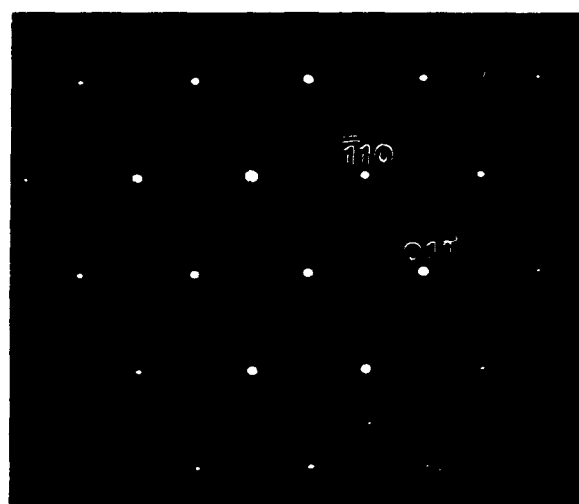


Fig. 12. Electron diffraction pattern from the $[111]$ zone axes showing the absence of spot splitting.

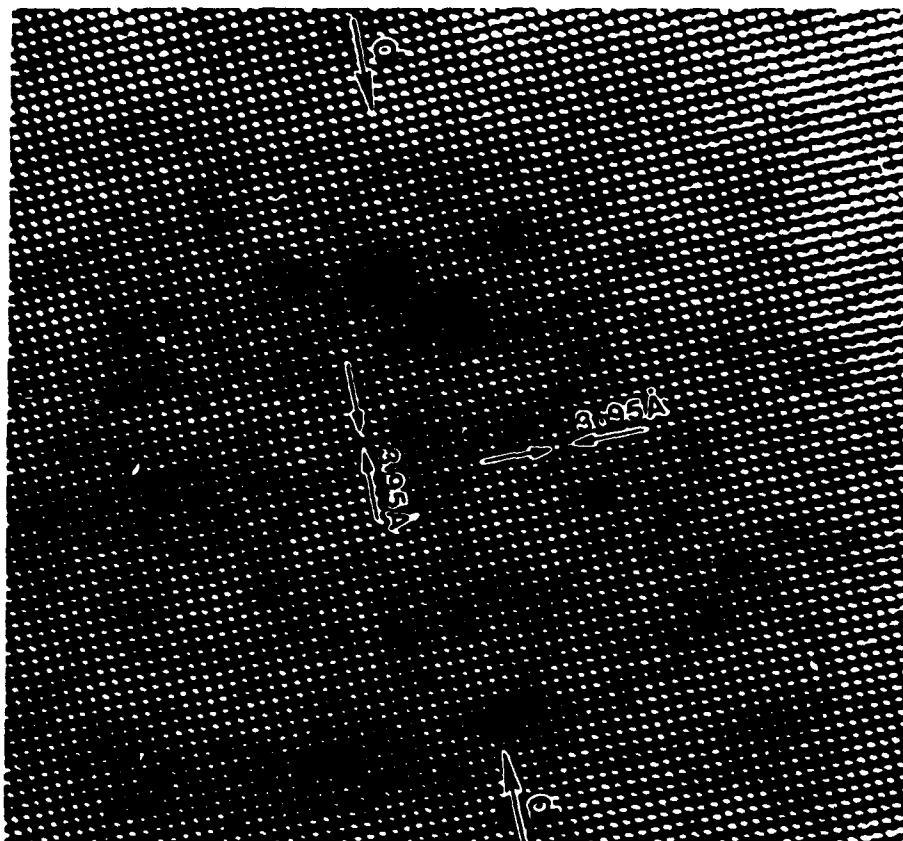


Fig. 13. High resolution electron micrograph showing no perceptible variation in lattice spacing across the domain boundary. The approximate position of the domain boundary is indicated by the arrows marked d.

*Submitted for publication to Journal of Materials
Science*

DIELECTRIC PROPERTIES AND MICROSTRUCTURAL CHARACTERIZATION OF

$(\text{Ba}_x\text{Ca}_{1-x})\text{TiO}_3$

Sudhakar Subrahmanyam and Edward Goo

Department of Materials Science and Engineering, University of Southern California

Los Angeles, CA 90089-0241

ABSTRACT

The microstructure of $(\text{Ba}_x\text{Ca}_{1-x})\text{TiO}_3$ ($0.0 \leq x \leq 0.2$) and ($0.8 \leq x \leq 1.0$) have been investigated by x-ray diffraction and transmission electron microscopy. The crystal structure at room temperature has been determined to be orthorhombic in the range ($0.0 \leq x \leq 0.2$) and tetragonal in the range ($0.8 \leq x \leq 1.0$). Ferroelectric domains have been observed by TEM in the Ba-rich compositions and the crystallography of the domains is consistent with a tetragonal crystal, similar to that in BaTiO_3 . An ordered structure is observed in the Ca-rich region, which is similar to that observed in the $(\text{Pb}_x\text{Ca}_{1-x}\text{TiO}_3)$ system. Dielectric studies do not reveal any relaxor behavior, however, the system exhibits diffuse phase transformations above room temperature (for $0.8 \leq x < 1.0$). It is observed that the sintering temperature has an effect on the dielectric properties. The diffuseness coefficient, δ , is determined from a semi-empirical method.

I. Introduction

Barium titanate is a widely used perovskite because of its high dielectric constant and excellent piezoelectric properties. Calcium titanate is also a perovskite-type material which is not ferroelectric at room temperature. Currently, there is a considerable interest in ferroelectric ceramics exhibiting diffuse phase transitions because of their unusual dielectric, electromechanical, and electro-optic behavior [1,2]. Substitution of other cations for Ti at the B site in BaTiO_3 has been extensively studied. Very little work has been done on A-site substituted perovskites.

A solid solution for $(\text{Ba}_x\text{Ca}_{1-x})\text{TiO}_3$ exists only in the composition range ($0.0 \leq x \leq 0.2$) and ($0.8 \leq x \leq 1.0$) [3] although little is known about these compositions [4]. The $(\text{Ba}_x\text{Ca}_{1-x})\text{TiO}_3$ is potentially an excellent system for dielectric and piezoelectric applications.

The paraelectric to ferroelectric phase transition is generally a very sharp transition. Complex perovskites have exhibited a gradual or diffuse phase transitions [5,6]. It has been suggested that the statistical composition fluctuations which must occur if crystallographically equivalent sites are occupied randomly by different cations [7] is the reason for the diffuse characteristics of the normally sharp transitions. Research in ordered perovskites is consistent with this model [8].

In the present study, the crystal structure and the microstructure in $(\text{Ba}_x\text{Ca}_{1-x})$

x)TiO₃ were studied by x-ray diffraction and transmission electron microscopy. The dielectric and hysteresis properties and ferroelectric phase transitions were also studied. In this paper, our observations on the effect of calcium titanate additions on the diffuse phase transitions in the (Ba_xCa_{1-x})TiO₃ system is presented using the power law model of Uchino *et al.* [9] in order to determine the diffuseness parameter, δ .

II. Experimental Procedure

The compositions of the samples were (Ba_xCa_{1-x})TiO₃, where x varied from 0.0 to 0.2 and 0.8 to 1.0 in 0.1 increments. The composition at $x = 0.5$, i.e. (Ba_xCa_{1-x})TiO₃ was also studied. These compositions refer to the relative amounts of oxides used in preparing the powder. Bulk processing of the perovskite powder was done with chemically pure CaCO₃ (99.5%), TiO₂ (99.7%), and BaCO₃ (99.5%). The powders were mixed by ball milling with alumina balls and distilled water (in the form of a slurry) for 5 hours in a polyethylene container and oven dried. The powder was then calcined in a covered alumina crucible at 850°C for 5 h. After remilling again for 5 h followed by drying, the final product was ground with a mortar and pestle into a fine powder. The powders were then cold pressed at a pressure of 240 MPa (35,000 psi) into disks 3 mm thick and 25 mm in diameter. The compacts were then sintered in a covered alumina dish packed with powders of the same composition at 1200°C

for 5 h. The compositions at $x = 0.8$ and 0.9 were also sintered at $1350\text{ }^{\circ}\text{C}$ for 5 h to study the effect of the sintering temperature on material properties.

X-ray samples were obtained by cutting a thin slice from the as-sintered samples and mechanically polishing with a final polish in $0.3\text{ }\mu\text{m}$ alumina slurry to give a smooth surface. Lattice parameters were measured by using a Rigaku X-ray diffractometer, using $\text{Cu K}\alpha$ radiation source, operating at 35 kV and 50 mA.

Transmission electron microscopy (TEM) samples were prepared by ultrasonically drilling the sintered samples into 3 mm disks. The disks were mechanically polished and dimpled to $20\text{ }\mu\text{m}$ and then ion-milled with argon ions at 5 kV and an incident angle of 18° . TEM was done on a Phillips EM 420 microscope operating at an accelerating voltage of 120 kV and using a double tilt stage.

Grain size measurements were done on a Cambridge Instruments Model 360 scanning electron microscope on the as-sintered surface. The samples for the dielectric measurements were obtained by cutting a thin slice from the as-sintered samples and mechanically polishing with a final polish in $0.3\text{ }\mu\text{m}$ alumina slurry to give a smooth surface, which was then coated with silver electrodes on both sides, using a Denton vacuum evaporator. The dielectric measurements were carried out by using an experimental set up that was specifically designed to carry out these measurements at high and low temperatures. The set up is shown in *Fig. 1*. The low temperature measurements were done by cooling the samples with liquid nitrogen.

A Keithley 3322 LCZ meter was used to measure the variation of dielectric constant with temperature with an applied field of 1V rms (without any bias) and a sampling time of 480-600 ms. Hysteresis measurements were done using an automated Hewlett-Packard system.

III. Results and Discussion

(1) Crystal Structure

It has been reported previously [10] that BaTiO_3 is tetragonal (with a c/a ratio of 1.029) and CaTiO_3 is orthorhombic at room temperature. In the present study, it has been verified that the crystal structure of $(\text{Ba}_x\text{Ca}_{1-x})\text{TiO}_3$ remains tetragonal over the composition range $0.8 \leq x \leq 1.0$ and is orthorhombic over the composition range $0 \leq x \leq 0.2$. The indexed x-ray diffraction peaks and their corresponding 2-theta values were used to calculate the lattice parameters using the method given by Parrish and Wilson [11]. The lattice parameters a and b increased with increasing barium content both in the orthorhombic and tetragonal regions while c decreased in the orthorhombic and increased in the tetragonal regions. This is in agreement with linearly interpolating the a and c values for CaTiO_3 and BaTiO_3 . The c/a ratio decreases with increasing barium content in the orthorhombic region. The cell

volume ($V = abc$) increases with increasing barium content, both in the orthorhombic and the tetragonal compositions. Additional peaks were seen (which were non-perovskite type) in the $x = 0.2$ composition, which could be due to the lack of formation of a complete solid solution, thereby giving rise to a secondary phase (*Fig. 2*). This could be due to the fact that $x = 0.2$ is close to the boundary of complete miscibility and non-miscibility [4]. The presence of a secondary phase, $\text{Ca}_4\text{Ti}_3\text{O}_{10}$, was later confirmed by transmission electron microscopy. Also, X-ray diffraction did not reveal any cation ordering. X-ray diffraction of $(\text{Ba}_{0.5}\text{Ca}_{0.5})\text{TiO}_3$ showed the presence of peaks resulting from both BaTiO_3 and CaTiO_3 (*Fig. 3*), confirming the absence of solid solution formation at this composition.

(2) Observation of Domain Structure by Transmission Electron Microscopy

Ferroelectric domains have been observed in the compositions $0.8 \leq x \leq 1.0$. 90° domain boundaries were prominently seen [*Fig. 4*]. The domain boundaries were observed with less frequency with increasing Ca-content. The 90° boundary walls lie on the $\{101\}$ planes, and tend to be straight. These are the strain-induced domains whose boundaries are planar and lie on well-defined crystallographic planes.

The SADP of the $\langle 100 \rangle$ zone axis from a sample with composition $x = 0.8$ shows spot splitting in the region of the 90° domains (*Fig. 5a*). *Fig. 5b* shows the dark

field image for $\vec{g} = (011)$ close to the $[100]$ zone axis region. The spot splitting is consistent with the presence of 90° domains. These domain boundaries were observed only in the Ba-rich compositions. The composition at $x = 0.8$ is confirmed to be ferroelectric by the presence of a distinct hysteresis loop (*Fig. 6*) at room temperature. This composition had a coercive field of 0.732 MV/m and a spontaneous polarization of $6.587 \mu\text{C}/\text{cm}^2$. This is comparable to that of BaTiO_3 , which has a spontaneous polarization of $26 \mu\text{C}/\text{cm}^2$.

Grain size measurements by SEM (*Fig. 7*) indicate that the grains were $15.0 \mu\text{m}$ for samples sintered at 1200°C and increased with increase in sintering temperature. Also, it was seen that the domain boundaries were observed with increasing frequency as the sintering temperature was increased. This was true for both $x = 0.9$ and 0.8 compositions. In the Ca-rich compositions, namely $x = 0.1$ and 0.2 , no domain boundaries were seen. Instead, the selected area diffraction patterns showed the presence of superlattice reflections along the three principal zone axis which were identical to those observed in $(\text{Pb}_x\text{Ca}_{1-x})\text{TiO}_3$ [12]. The electron diffraction patterns for the $[100]$ zone axis contained both the $1/2\{100\}$ superlattice reflections alone, and the $1/2\{100\}$ and $1/2\{110\}$ superlattice reflections together. These reflections were indexed in terms of the perovskite unit cell, unless stated otherwise. Similarly, the electron diffraction pattern for the $[111]$ zone axis showed $1/2\{110\}$ superlattice reflections in all three directions, in two directions and in one direction

only. This may be explained if the reflections arise from different variants. The [110] zone axis diffraction pattern showed the presence of $1/2\{111\}$ reflections alone, and also the $1/2\{100\}$ and $1/2\{111\}$ reflections together. The calcium titanate structure is a regular TiO_6 octahedra rotated with respect to their ideal perovskite positions as shown in Fig. 8 [13,14]. This occurs primarily due to the small displacements of the calcium and oxygen atoms from their ideal lattice positions. The presence of superlattice reflections due to such displacements is revealed by TEM studies on CaTiO_3 .

The model proposed by King *et al.* [12] explained the reflections seen in $(\text{Pb}_x\text{Ca}_{1-x})\text{TiO}_3$ close to $x = 0.5$ for which an ordered structure was proposed. Chemical ordering of barium and calcium atoms account for the presence of $1/2\{111\}$ superlattice reflections and atomic shuffles or electrical ordering is responsible for the presence of $1/2\{100\}$ and $1/2\{110\}$ reflections. Atomic shuffles occur when a crystal transforms into an antiferroelectric state, leading to electrical ordering¹². Since CaTiO_3 is antiferroelectric, atomic shuffles similar to that observed in pure CaTiO_3 is responsible for the presence of $1/2\{110\}$ and $1/2\{100\}$ superlattice reflections in $(\text{Ba}_x\text{Ca}_{1-x})\text{TiO}_3$. This is further confirmed by the fact that both $(\text{Pb}_x\text{Ca}_{1-x})\text{TiO}_3$ and $(\text{Sr}_x\text{Ca}_{1-x})\text{TiO}_3$ [15] also show superlattice reflections identical to $(\text{Ba}_x\text{Ca}_{1-x})\text{TiO}_3$, however, no superlattice reflections are seen in the $(\text{Pb}_x\text{Ba}_{1-x})\text{TiO}_3$ [16] and $(\text{Pb}_x\text{Sr}_{1-x})\text{TiO}_3$ [17] systems.

There were a few regions in the Ca-rich side which showed non-perovskite type reflections (*Figs. 9*). These reflections could be due to the presence of a secondary phase, $\text{Ca}_4\text{Ti}_3\text{O}_{10}$ [18] as indicated by the XRD peaks. This is supported by the fact that two major X-ray peaks of this phase (at $\Theta \approx 33^\circ$ and 47°) corresponds to that seen in the present system. The EDS spectra from these regions (*Fig. 10*) do not show the presence of any Ba peak, which gives further evidence that these regions may be a secondary phase of CaTiO_3 . The $\text{Ca}_4\text{Ti}_3\text{O}_{10}$ phase is orthorhombic with $a = 3.827 \text{ \AA}$, $b = 27.15 \text{ \AA}$ and $c = 7.094 \text{ \AA}$.

(3) Dielectric Measurements

The $(\text{Ba}_x\text{Ca}_{1-x})\text{TiO}_3$ system exhibits a diffuse phase transition (Curie point) above room temperature over the composition range $0.8 \leq x \leq 1.0$. (*Fig. 11*). Just as BaTiO_3 shows a paraelectric to ferroelectric transformation at 120°C (Curie point) and another phase transformation from tetragonal to orthorhombic at 5°C , it is seen that $(\text{Ba}_x\text{Ca}_{1-x})\text{TiO}_3$ shows two transformations, one diffuse transformation above room temperature and one sharp transformation below room temperature (*Table I*).

The addition of calcium to barium titanate shifts the Curie temperature beyond 120°C (that of BaTiO_3) and gives rise to diffuse phase transformations

Table I : Transformation Temperatures of $(\text{Ba}_x\text{Ca}_{1-x})\text{TiO}_3$

$(\text{Ba}_x\text{Ca}_{1-x})\text{TiO}_3$	Cubic to Tetragonal (T_c) (°C)	Tetragonal to Orthorhombic (°C)
$x = 1.0$	120	5
$x = 0.9$	143	15
$x = 0.8$	136	11

above room temperature [19]. The sharpness of the tetragonal - orthorhombic transformation could be due to the formation of moisture while cooling in liquid nitrogen. Since there were no dopants added, the dielectric loss was significant. The dielectric loss increased at lower frequencies, resulting in higher values for the dielectric constant.

It was observed that the dielectric curves for the samples that were sintered at 1350 °C were sharper and higher than for those sintered at 1200 °C. The peak value of the dielectric constant was higher in the 1350 °C case, and the peaks were less diffuse (Fig. 12). It is well known that grain size has a pronounced effect on the dielectric properties [20]. Effect of chemical purity, preparation procedure, initial particle size distribution of the powder, final grain size distribution, resistivity of the grains and the grain boundaries and the density of the ceramic etc. should be considered as external contributions to the dielectric anomaly.

The temperature dependence of the dielectric constant for a relaxor dielectric at a fixed frequency can be described by the semi-empirical relationship given by

Smolenskii [6]:

$$\frac{1}{k^x} = \frac{1}{k_{\max}^x} + \frac{(T-T_c)^2}{2\delta_x^2 k_{\max}^x} \quad (1)$$

where k^x = dielectric constant,

k_{\max}^x = maximum dielectric constant,

T_c = Curie point,

and δ_x = diffuseness coefficient

The modified form of the above equation was given as [21]: (2)

$$\frac{1}{k} = \frac{1}{k_{\max}} \left[1 + \frac{(T-T_c)^\gamma}{2\delta^2} \right] (1 \leq \gamma \leq 2)$$

where γ is an empirical term which is equal to 1 for ideal Curie-Weiss law behavior and is equal to 2 for ideal relaxor behavior and has intermediate values for all other materials. In order to determine the diffuseness parameter δ_x , the exponent γ was obtained from the slope of $\ln[k_{\max}/k - 1]$ vs $\ln[T-T_c]$, using a least square fit (*Fig. 13*). Then, the diffuseness parameter δ_x was obtained from the slope of the plot of $1/k$ vs $[T-T_c]^\gamma$ (*Fig. 14*), using a least square fit (*Table II*). Since γ is a purely empirical term, a value less than one is not unusual, even though, ideally γ has values ranging between one and two.

Smolenskii [6]:

$$\frac{1}{k^\gamma} = \frac{1}{k_{\max}^\gamma} + \frac{(T-T_c)^2}{2\delta_x^2 k_{\max}^\gamma} \quad (1)$$

where k^γ = dielectric constant,

k_{\max}^γ = maximum dielectric constant,

T_c = Curie point,

and δ_x = diffuseness coefficient

The modified form of the above equation was given as [21]: (2)

$$\frac{1}{k} = \frac{1}{k_{\max}} \left[1 + \frac{(T-T_c)^\gamma}{2\delta^2} \right] (1 \leq \gamma \leq 2)$$

where γ is an empirical term which is equal to 1 for ideal Curie-Weiss law behavior and is equal to 2 for ideal relaxor behavior and has intermediate values for all other materials. In order to determine the diffuseness parameter δ_x , the exponent γ was obtained from the slope of $\ln[k_{\max}/k - 1]$ vs $\ln[T-T_c]$, using a least square fit (*Fig. 13*). Then, the diffuseness parameter δ_x was obtained from the slope of the plot of $1/k$ vs $[T-T_c]^\gamma$ (*Fig. 14*), using a least square fit (*Table II*). Since γ is a purely empirical term, a value less than one is not unusual, even though, ideally γ has values ranging between one and two.

TABLE II
Physical and Electrical Properties of $(\text{Ba}_x\text{Ca}_{1-x})\text{TiO}_3$

Composition x	0	0.1	0.2	0.8	0.9	1.0
Molecular Weight (gms)	135.88	145.61	155.34	213.73	223.46	223.20
$a(\text{\AA})$	5.381	5.456	5.470	3.973	3.991	3.999
$b(\text{\AA})$	7.645	7.668	7.680	3.973	3.991	3.999
$c(\text{\AA})$	5.443	5.393	5.379	4.006	4.013	4.039
c/a	1.0115	0.9884	0.9833	1.0083	1.0055	1.0100
Cell Volume (\AA^3)	223.912	225.624	225.969	63.233	63.919	64.591
Curie Point ($^{\circ}\text{C}$)	-	-	-	136	143	120
Dielectric Constant (RT)	100	-	-	400	1000	2800
Resistivity (ρ)	-	3.37 M	0.94 M	1.64 M	7.87 M	-
Diffuseness Parameter, δ_s	-	-	-	260	2993	15
Exponent, γ	-	-	-	1.358	2.001	1.17

IV. Conclusion

Crystal structure and domain structure of $(\text{Ba}_x\text{Ca}_{1-x})\text{TiO}_3$, with x ranging from 0.0 to 0.2 and 0.8 to 1.0 were investigated by x-ray diffraction and transmission electron microscopy. The crystal structure was determined to be tetragonal for $x \geq 0.8$ and orthorhombic for $x \leq 0.2$. 90° domains were prominently observed in the Ba-rich compositions, which were oriented along the $\{101\}$ crystallographic plane

consistent with the tetragonal symmetry. The measurement of dielectric properties for x ranging from 0.8 to 1.0 indicated the presence of two phase transformations with no frequency dependence, thereby exhibiting no relaxor behavior. The transition above room temperature at the Curie point was a diffuse phase transition while the transition below room temperature was sharp. The sintering temperature was observed to have an effect on the nature of the dielectric curves and also the grain size. The diffuseness parameter, δ_u , was calculated using a semi-empirical relation.

Acknowledgements: The authors acknowledge the use of the facilities at the Center for Electron Microscopy and Microanalysis (CEMMA) at USC. The authors would also like to acknowledge Dr. Clive Randall and Mr. V. Sundar of the Materials Research Laboratory, The Pennsylvania State University, for useful discussions and assistance in the hysteresis measurements. This work was supported by the Office of Naval Research under Grant No. N00014-90-J-1900.

References

1. G. Schmidt, *Phase Trans.* **20** (1990) 127.
2. L.E. Cross, *Ferroelectrics* **76** (1987) 241.
3. T. Ikeda, *J. Phys. Soc. Japan* **13** (1958) 335.
4. G. Dyrst, M. Grotenhuis, and A. G. Barkow, *J. Am. Ceram. Soc.* **33** (1950) 231.
5. D. Hennings, A. Schnell, G. Simon, *J. Am. Ceram. Soc.* **65** (1982) 539.
6. G. A. Smolenskii, *J. Phys. Soc. Jpn.* **28 Suppl.** (1970) 26.
7. N. Setter, *J. Mater. Sci.*, **15** (1980) 2478.
8. B. N. Rolov, *Sov. Phys. Solid State* **6** (1965) 1676.
9. K. Uchino and S. Nomura, *Ferroelectric Lett.* **44** (1982) 55.
10. F. S. Galasso, "Structure, Properties and Preparation of Perovskite-Type Compounds" (Pergamon Press, Oxford, 1969).
11. W. Parrish and A. J. C. Wilson, in *International Tables for X-ray Crystallography*, Vol. 2, edited by J. S. Kasper and K. Lonsdale (The Kynoch Press, Birmingham, England, 1959).
12. Grace King, Edward Goo, Takashi Yamamoto and Kiyoshi Okazaki, *J. Am. Ceram. Soc.* **71** (1988) 454.
13. H. F. Kay and P. C. Bailey, *Acta Cryst.* **10** (1957) 219.
14. H. G. A. Koopmans, G. M. H. Van De Velde and P. J. Gellings, *Acta Cryst. C*

- 39 (1983) 1323.
15. Grace King, Ph.D. Thesis, University of Southern California (1990).
 16. S. Subrahmanyam, R. Ganesh and E. Goo, *Ceram. Trans.* **32** (1992) 139.
 17. K. Ananth, R. Ganesh and E. Goo, *Ceram. Trans.* **32** (1992) 145.
 18. Roth, *J. Res. Natl. Bur. Stand. (U.S.)* **61** (1958) 437.
 19. P. S. R. Krishna, Dhananjai Pandey, V.S. Tiwari, R. Chakravarthy and B.A. Dasannacharya, *Appl. Phys. Lett.* **62** (1993) 231.
 20. U. Kumar, S. F. Wang, S. Varanasi and J. P. Dougherty, in *Proceedings of the 8th IEEE International Symposium on Applications of Ferroelectrics* (1992) p. 55.
 21. K. Uchino and S. Nomura, *Ferroelectr. Lett.* **44** (1982) 55.

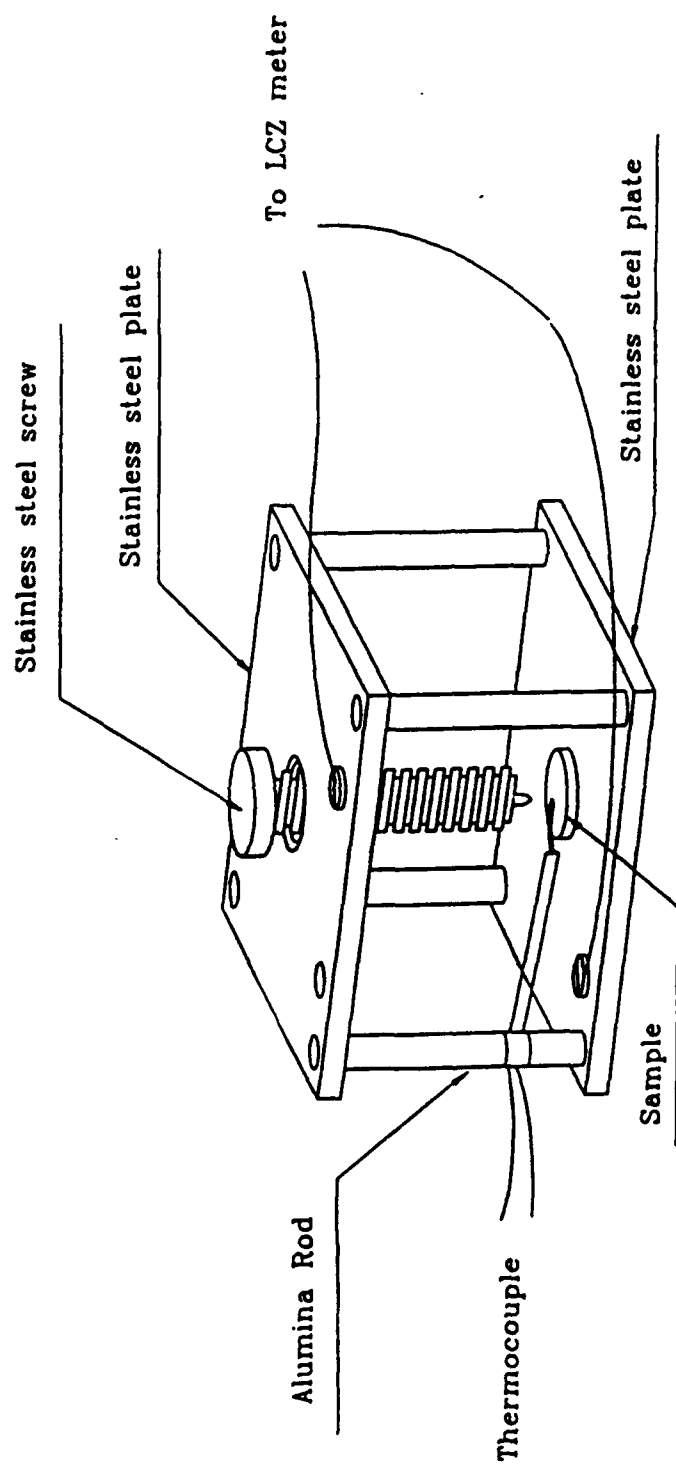


Fig. 1. A schematic of the dielectric set-up used in the present experiments for high-temperature measurements.

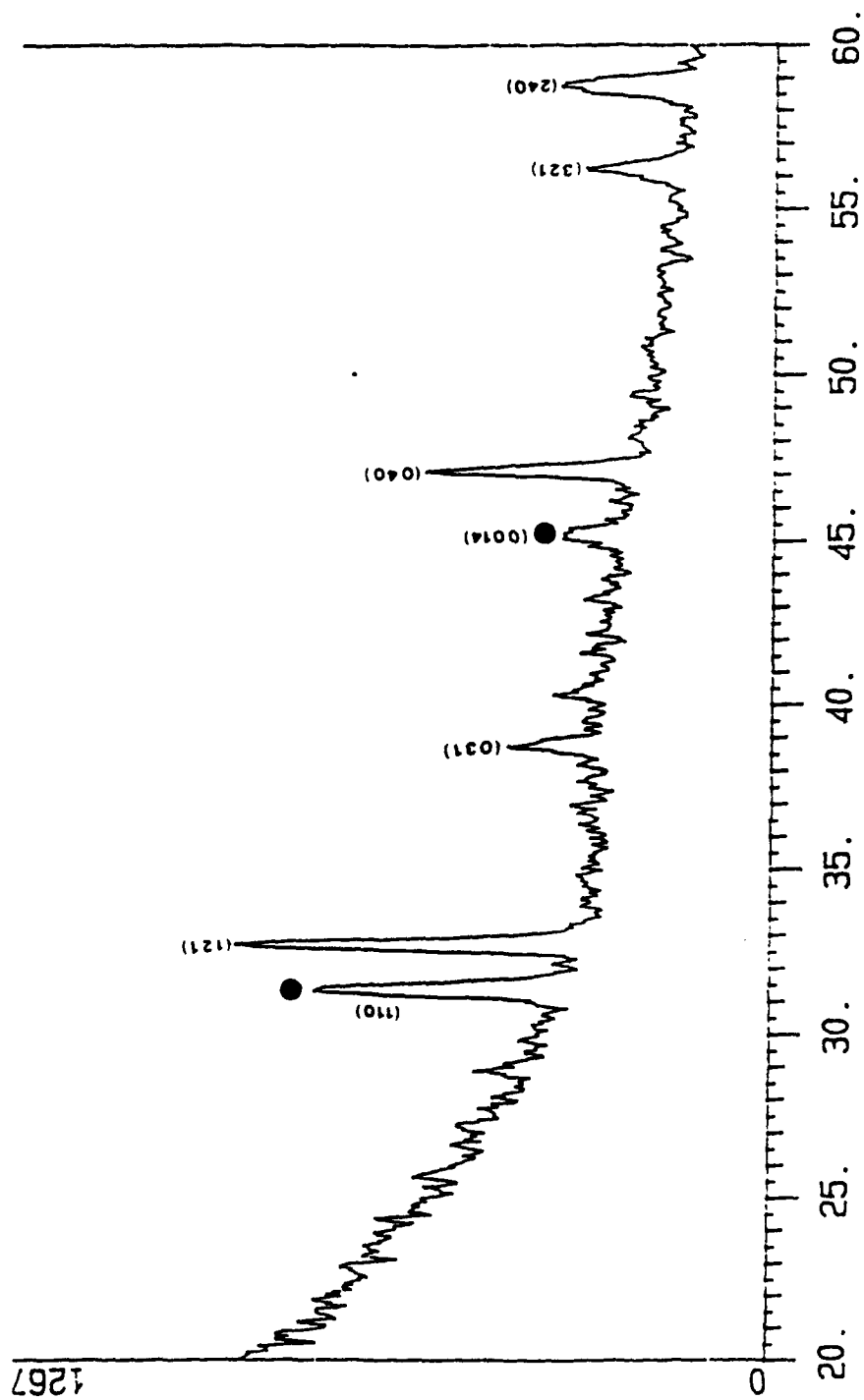


Fig. 2. X-ray diffraction pattern showing a secondary phase (●) of $\text{Ca}_4\text{Ti}_3\text{O}_{10}$ in $(\text{Ba}_{0.2}\text{Ca}_{0.8})\text{TiO}_3$.

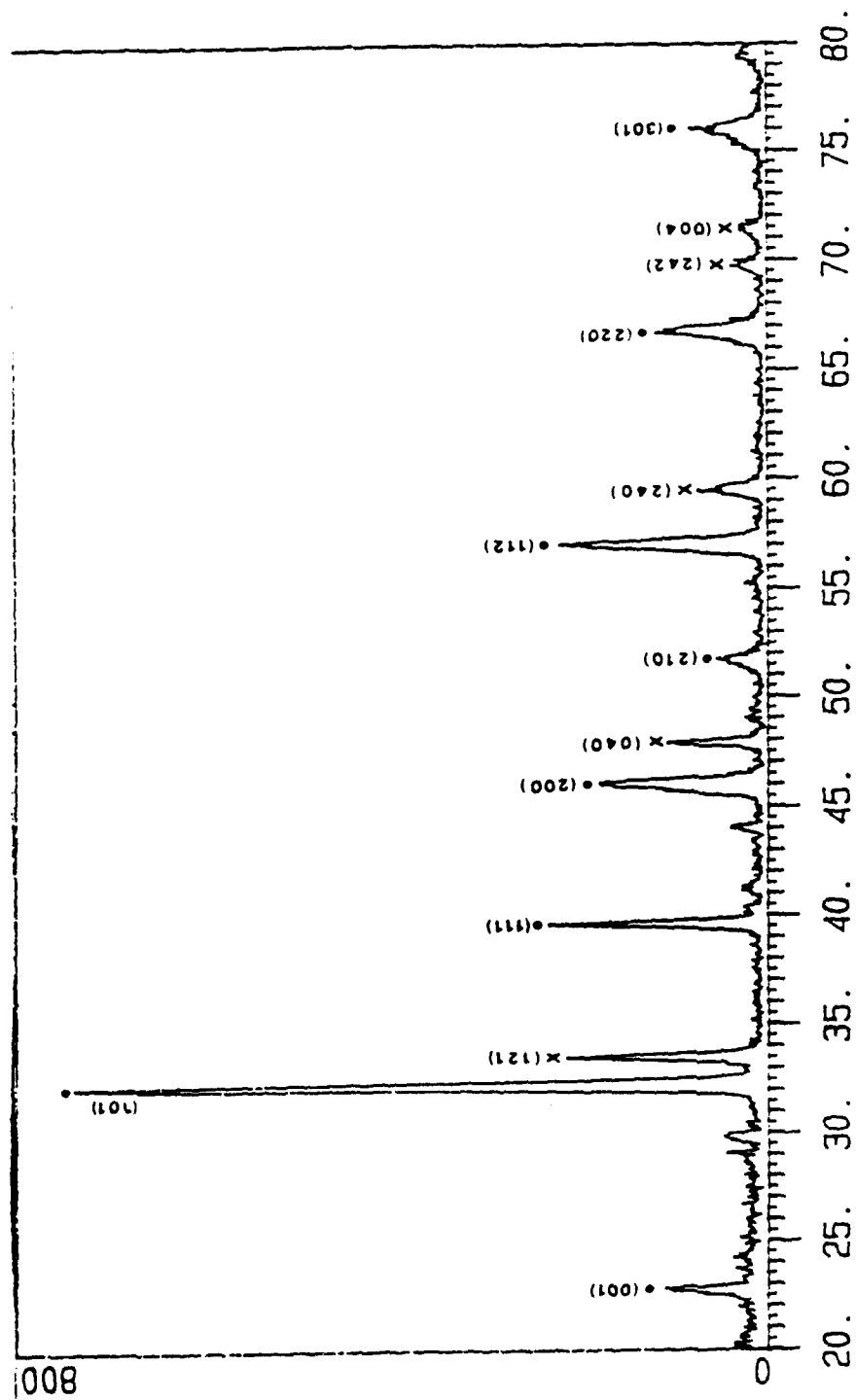


Fig. 3. X-ray diffraction of $(\text{Ba}_{0.5}\text{Ca}_{0.5})\text{TiO}_3$ showing peaks from both BaTiO_3 (X) and CaTiO_3 (•) due to the lack of a solid solution formation.

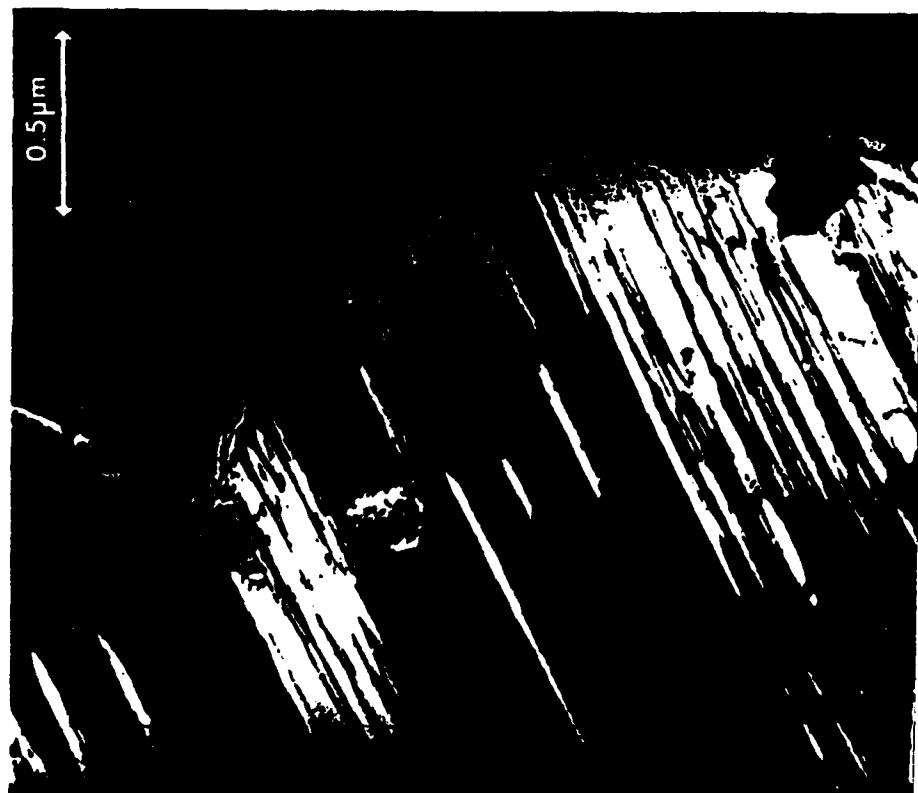


Fig. 4. Dark field micrograph taken ($x = 0.9$) with $\{\bar{1}10\}$ type reflection from $[100]$ zone axis showing the 90° domain walls oriented along the (101) plane.

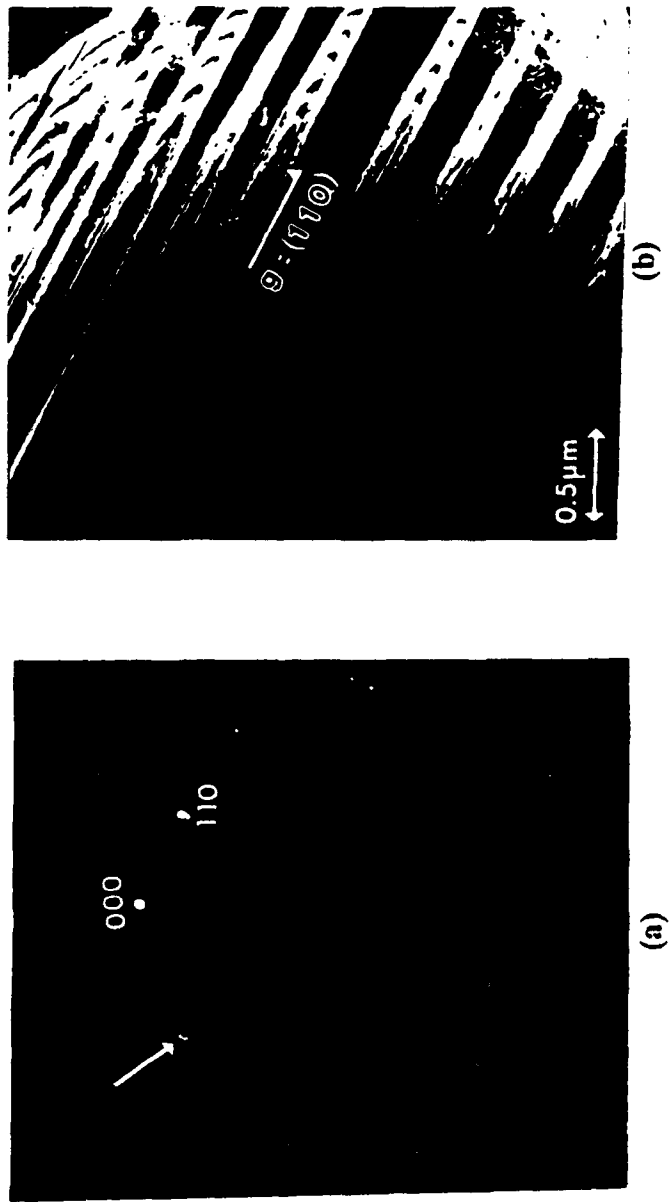


Fig. 5. (a) The two beam condition from the $\{110\}$ type reflection in the $[100]$ zone axis, showing spot splitting in the region of the 90° domains.

(b) Dark-field of the same region.

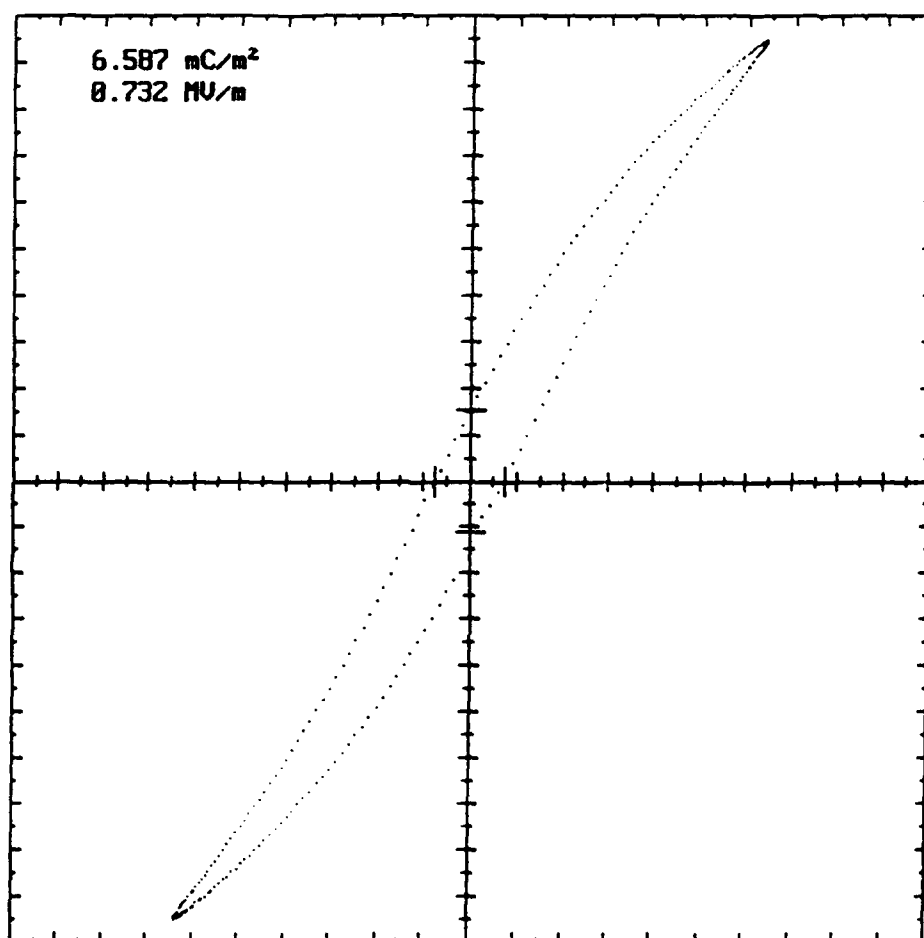
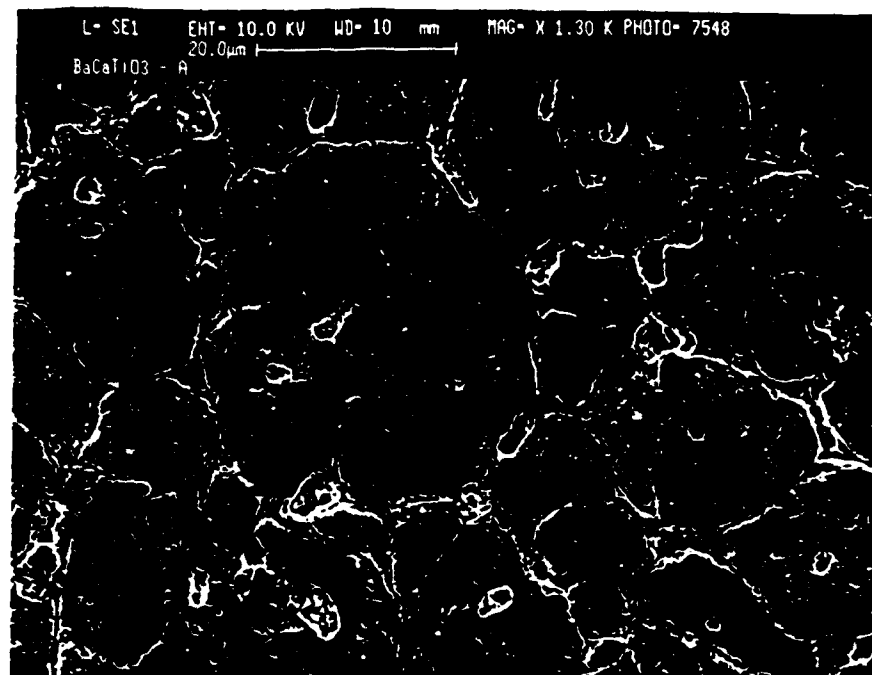
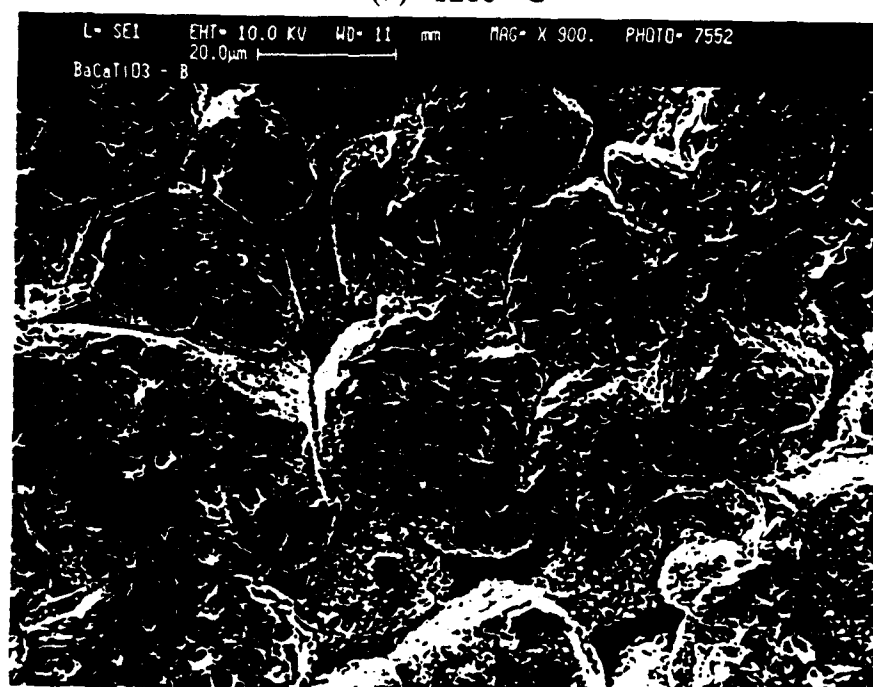


Fig. 6. A distinct hysteresis loop in the $(\text{Ba}_{0.3}\text{Ca}_{0.2})\text{TiO}_3$ composition confirming its ferroelectric nature (Scale : x-axis : 1 div = 0.5 MV/m; y-axis : 1 div = 2.5 mC/m²).



(a) 1200 °C



(b) 1350 °C

Fig. 7. Grain distribution in $(\text{Ba}_{0.9}\text{Ca}_{0.1})\text{TiO}_3$ (a) sintered at 1200 °C and (b) sintered at 1350 °C.

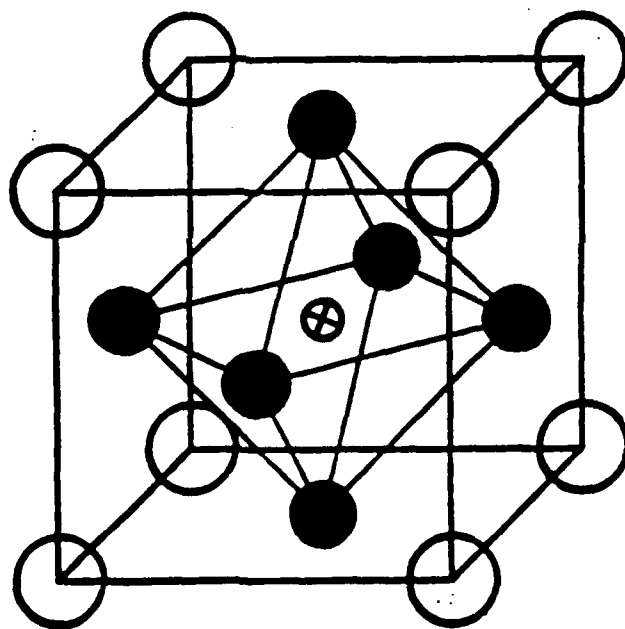


Fig. 8. The structure of calcium titanate is a regular TiO_6 octahedra rotated with respect to their ideal perovskite positions [13,14].

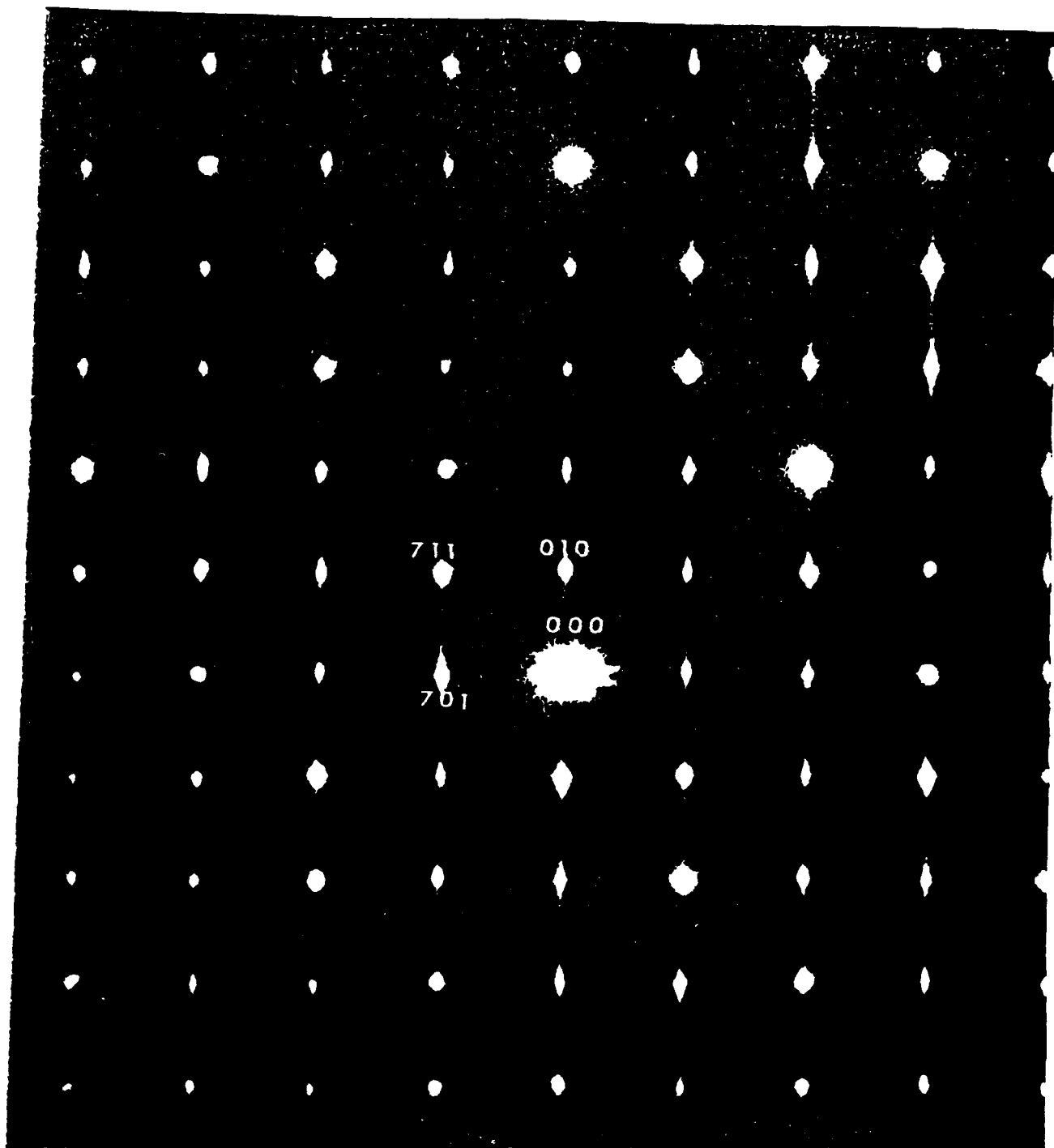


Fig. 9. The $\langle 10\bar{7} \rangle$ zone axis of the orthorhombic secondary phase of $\text{Ca}_2\text{Ti}_2\text{O}_7$.

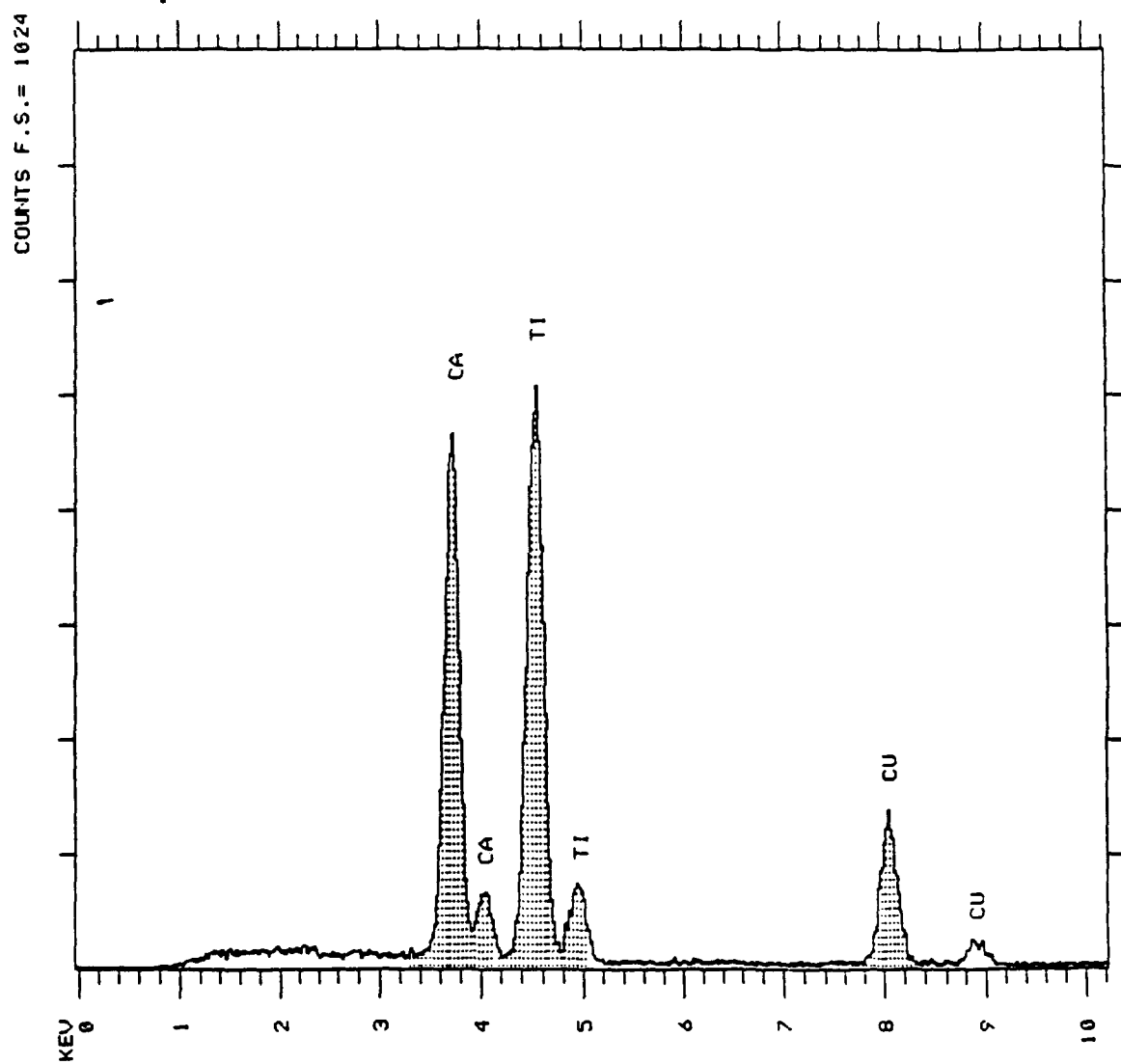


Fig. 10. EDS spectra from the region of non-perovskite reflections showing the absence of Ba peaks.

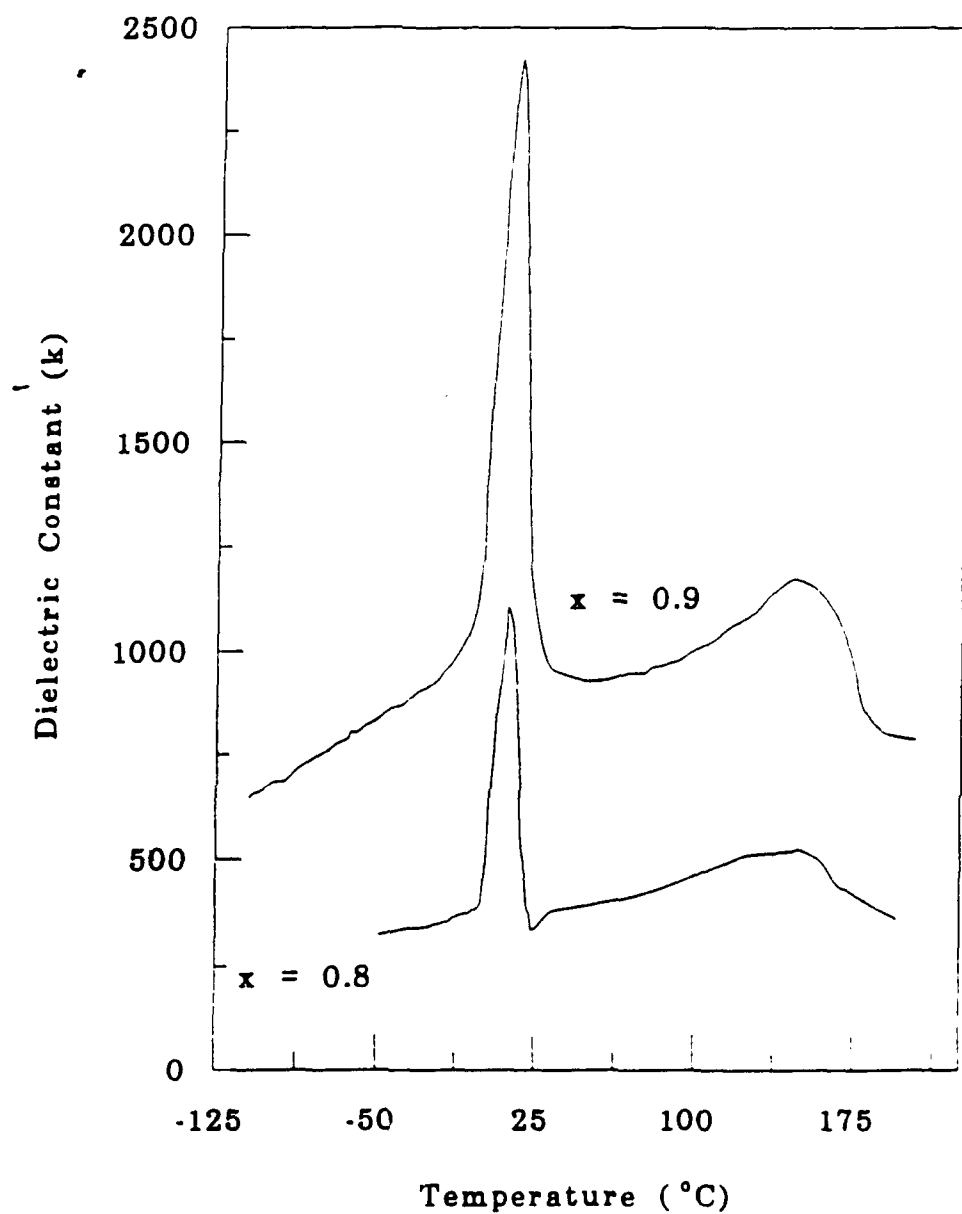
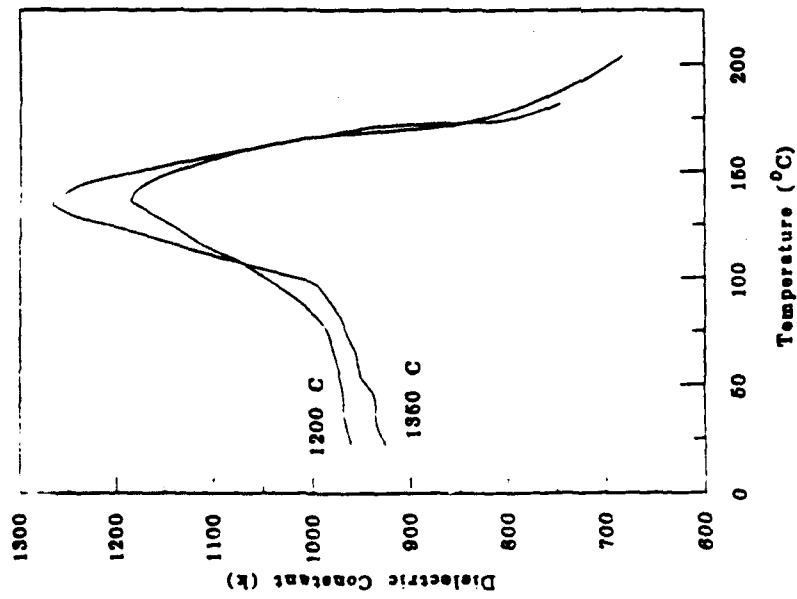
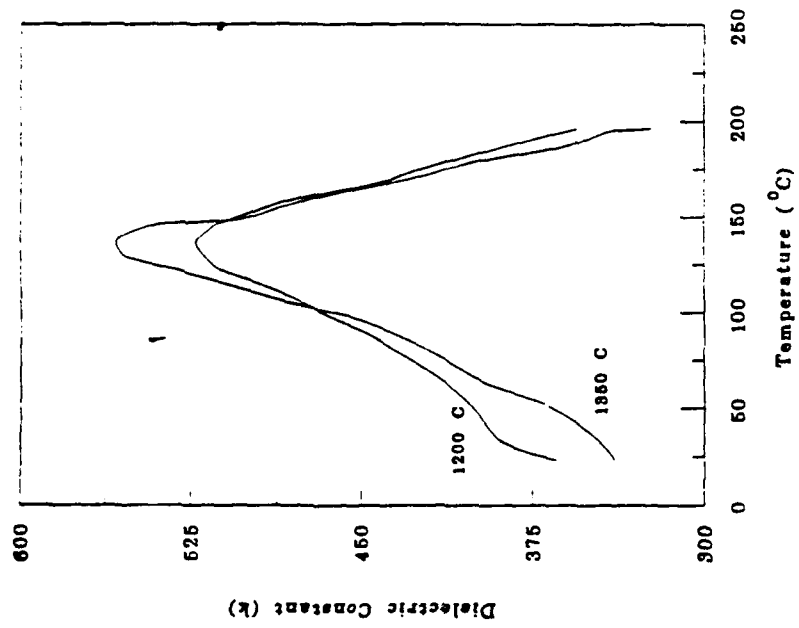


Fig. 11. The variation of dielectric constant (at 10 kHz) with temperature for the $(\text{Ba}_x\text{Ca}_{1-x})\text{TiO}_3$ system for $x = 0.9$ and 0.8 .



(a) $(\text{Ba}_{0.9}\text{Ca}_{0.1})\text{TiO}_3$



(b) $(\text{Ba}_{0.9}\text{Ca}_{0.1})\text{TiO}_3$

Fig. 12. The effect of sintering temperature on the dielectric curves for $(\text{Ba}_x\text{Ca}_{1-x})\text{TiO}_3$

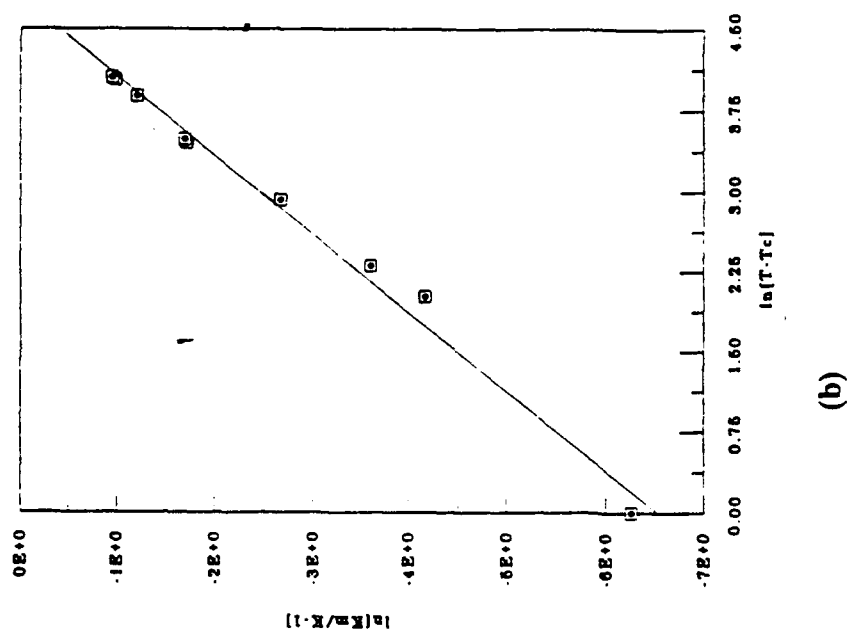
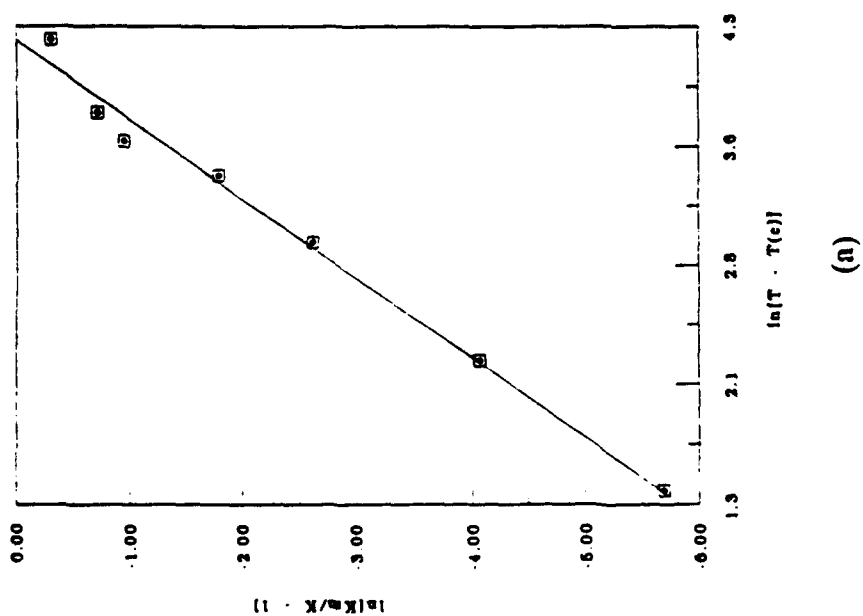
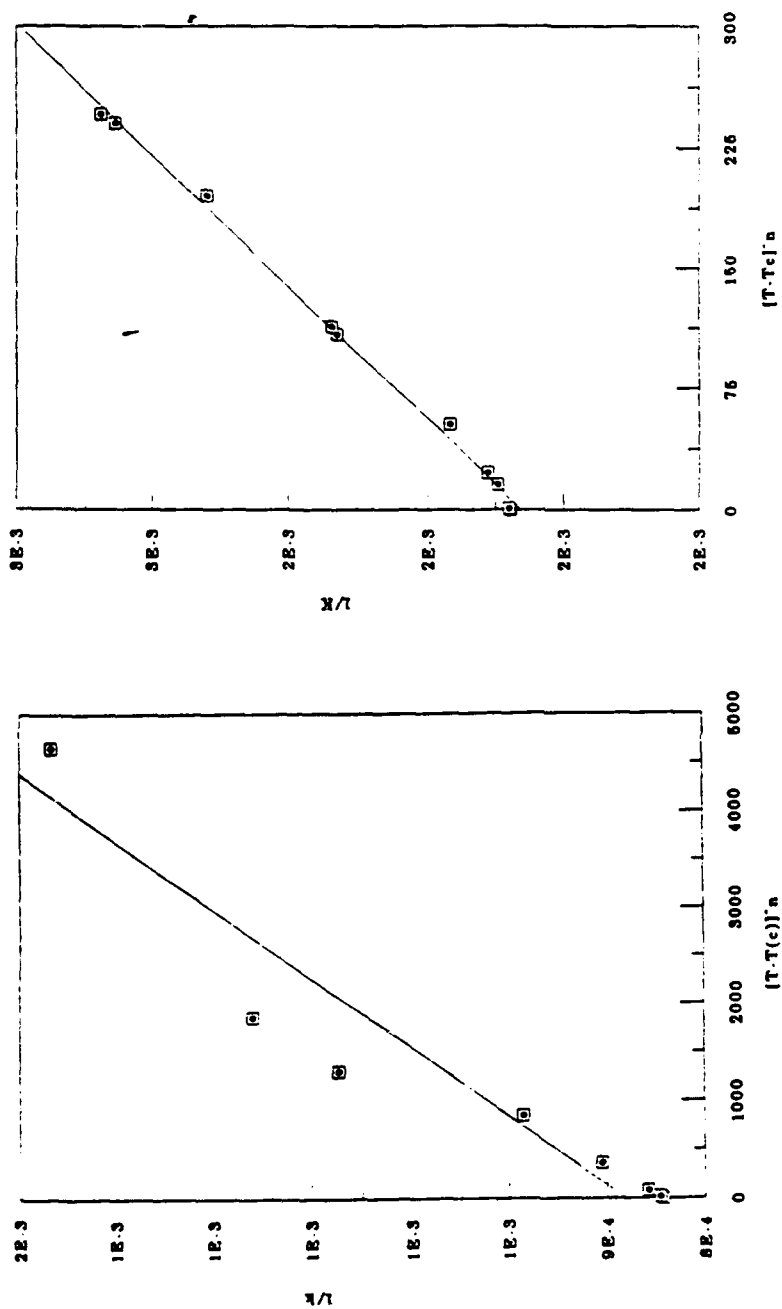


Fig. 13. Determination of the exponent γ for (a) $\text{Ba}_{0.9}\text{Ca}_{0.1}\text{TiO}_3$ and (b) $\text{Ba}_{0.8}\text{Ca}_{0.2}\text{TiO}_3$.



(a)

(b)

Fig. 14. Determination of the diffuseness parameter δ_x for (a) $\text{Ba}_{0.9}\text{Ca}_{0.1}\text{TiO}_3$ and (b) $\text{Ba}_{0.8}\text{Ca}_{0.2}\text{TiO}_3$.

List of Figures

- Fig. 1.* A schematic of the dielectric set-up used in the present experiments for high-temperature measurements.
- Fig. 2.* X-ray diffraction pattern showing a secondary phase (●) of $\text{Ca}_4\text{Ti}_3\text{O}_{10}$ in $(\text{Ba}_{0.2}\text{Ca}_{0.8})\text{TiO}_3$.
- Fig. 3.* X-ray diffraction of $(\text{Ba}_{0.5}\text{Ca}_{0.5})\text{TiO}_3$ showing peaks from both BaTiO_3 (X) and CaTiO_3 (●) due to the lack of a solid solution formation.
- Fig. 4.* Dark field micrograph taken ($x = 0.9$) with $\{\bar{1}10\}$ type reflection from $[100]$ zone axis showing the 90° domain walls oriented along the (101) plane.
- Fig. 5. (a)* The two beam condition from the $\{110\}$ type reflection in the $[100]$ zone axis, showing spot splitting in the region of the 90° domains.
(b) Dark-field of the same region.
- Fig. 6.* A distinct hysteresis loop in the $(\text{Ba}_{0.8}\text{Ca}_{0.2})\text{TiO}_3$ composition confirming its ferroelectric nature (Scale : x-axis : 1 div = 0.5 MV/m; y-axis : 1 div = 2.5 mC/m²).
- Fig. 7.* Grain distribution in $(\text{Ba}_{0.9}\text{Ca}_{0.1})\text{TiO}_3$ (a) sintered at 1200 °C and (b) sintered at 1350 °C.
- Fig. 8.* The structure of calcium titanate is a regular TiO_6 octahedra rotated with respect to their ideal perovskite positions [13,14].

Fig. 9. The $\langle 10\bar{7} \rangle$ zone axis of the orthorhombic secondary phase of $\text{Ca}_4\text{Ti}_3\text{O}_{10}$.

Fig. 10. EDS spectra from the region of non-perovskite reflections showing the absence of Ba peaks.

Fig. 11. The variation of dielectric constant (at 10 kHz) with temperature for the $(\text{Ba}_x\text{Ca}_{1-x})\text{TiO}_3$ system for $x = 0.9$ and 0.8 .

Fig. 12. The effect of sintering temperature on the dielectric curves for $(\text{Ba}_x\text{Ca}_{1-x})\text{TiO}_3$.

Fig. 13. Determination of the exponent γ for (a) $\text{Ba}_{0.9}\text{Ca}_{0.1}\text{TiO}_3$ and (b) $\text{Ba}_{0.8}\text{Ca}_{0.2}\text{TiO}_3$.

Fig. 14. Determination of the diffuseness parameter δ_x for (a) $\text{Ba}_{0.9}\text{Ca}_{0.1}\text{TiO}_3$ and (b) $(\text{Ba}_{0.8}\text{Ca}_{0.2})\text{TiO}_3$.